Journal of Materials Chemistry A

Accepted Manuscript

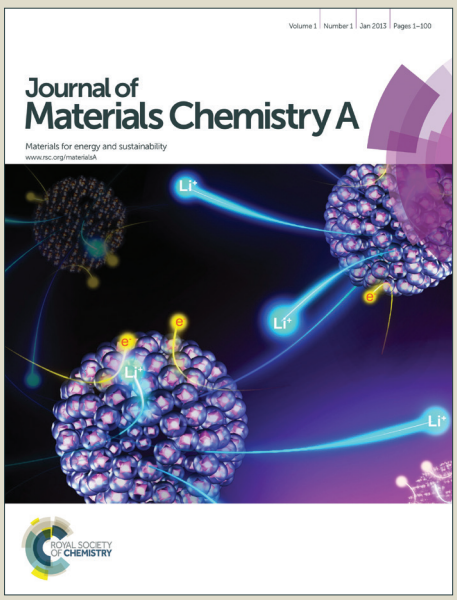

ROYAL SOCIETY OF CHEMISTRY

www.rsc.org/materialsA

WO_3 based solid solution oxide – Promising Proton Exchange Membrane Fuel Cell Anode Electro-catalyst

Prasad Prakash Patel[1], Prashanth H. Jampani[2], Moni Kanchan Datta[2,3], Oleg Velikhokhatnyi[2,3], Daeho Hong[2], James A. Poston[4], Ayyakkannu Manivannan[4], Prashant N. Kumta[1,2,3,5*]

[1]Department of Chemical and Petroleum Engineering, Swanson School of Engineering, University of Pittsburgh, Pittsburgh, PA 15261, USA.

[2]Department of Bioengineering, Swanson School of Engineering, University of Pittsburgh, Pittsburgh, PA 15261, USA.

[3]Center for Complex Engineered Multifunctional Materials, University of Pittsburgh, PA 15261, USA.

[4]US Department of Energy, National Energy Technology Laboratory, Morgantown, WV 26507.

[5]Mechanical Engineering and Materials Science, Swanson School of Engineering, University of Pittsburgh, Pittsburgh, PA 15261, USA.

[*]Corresponding author: Prashant N. Kumta (pkumta@pitt.edu)

Department of Bioengineering, 815C Benedum Hall, 3700 O'Hara Street, Pittsburgh, PA 15261.

Tel: +1-412-648-0223, Fax: +1-412-624-3699

This is an abstract presented at the 2014 AIChE annual meeting in Atlanta, GA (November 16-21, 2014).

Highlights

- WO_3 based electro-catalysts–promising hydrogen oxidation reaction (HOR) catalyst for PEMFCs.
- W-Ir-O solid solution exhibits superior electrochemical response following DFT calculations.
- WO_3-IrO_2 solid solution show comparable electrochemical performance to state of the art Pt based electro-catalyst based on DFT studies.
- DFT calculations indicate IrO_2 introduction modify the electronic structure of WO_3.
- Nanostructured $(W_{1-x}Ir_x)O_y$ (x=0.2, 0.3) synthesized using a wet chemical approach.
- Electrochemical activity of $(W_{1-x}Ir_x)O_y$ (x=0.2, 0.3) for HOR as PEMFC anode was studied.
- $(W_{0.7}Ir_{0.3})O_y$ shows significantly improved electrochemical performance in contrast to WO_3.
- $(W_{0.7}Ir_{0.3})O_y$ shows comparable electrochemical performance to state of the art 40% Pt/C.
- $(W_{0.7}Ir_{0.3})O_y$ also shows comparable electrochemical stability/durability to Pt/C.

Abstract

There is a vital need to develop novel non-noble metals based electro-catalyst or reduced noble metal containing electro-catalyst with excellent electrochemical activity and stability fostering economic commercialization of proton exchange membrane fuel cells (PEMFCs). It is hence of paramount importance to identify and generate reduced noble metal containing electro-catalysts with high electrochemical active surface area, offering noble metal loadings in the ultra-low levels thus reducing the overall PEMFCs capital costs. Using theoretical first principles d-band center calculations of tungsten oxide (WO_3) based electro-catalysts containing IrO_2 as a solute

for hydrogen oxidation reaction (HOR), we have identified, synthesized and experimentally demonstrated a highly active nanostructured $(W_{1-x}Ir_x)O_y$ (x=0.2, 0.3; y=2.7-2.8) electro-catalyst for HOR. Furthermore, experimental studies validate superior electrochemical activity of nanostructured $(W_{0.7}Ir_{0.3})O_y$ for HOR exhibiting improved/comparable stability/durability contrasted to pure WO_3 nanoparticles (WO_3-NPs), IrO_2 nanoparticles (IrO_2-NPs) as well as state of the art commercial 40% Pt/C system. Optimized composition of $(W_{0.7}Ir_{0.3})O_y$ was identified exhibiting ~33% higher and almost similar catalytic activity for HOR compared to IrO_2-NPs and commercial 40% Pt/C, respectively. Additionally, $(W_{0.7}Ir_{0.3})O_y$ showed significant enhancement in electrochemical activity for HOR compared to pure WO_3-NPs. Long-term life cycle test of $(W_{0.7}Ir_{0.3})O_y$ for 24 h also showed comparable electrochemical stability/durability compared to that of 40% Pt/C and pure WO_3-NPs. The results of half and full cell electrochemical characterization bode well with the theoretical studies demonstrating the promise of the WO_3 solid solution electro-catalyst.

Keywords

PEM fuel cells; Electro-catalyst; Hydrogen oxidation; Tungsten trioxide; Iridium oxide; Solid solution; Nanostructured; Hydrogen tungsten bronze

1. Introduction

Energy has been the subject of much debate and the highlight of much anticipated research over the past decade. Efficient use of energy and exploration of renewable and clean energy sources with no adverse environmental effects has been the focus of intense research activity conducted all over the globe in order to meet the growing demand of electric power.[1-4] Amidst the manifold research advances made, fuel cell technology has been hailed as one of the pervading and yet promising technology available for the continuous production of power with reduced greenhouse gas emissions, and portending higher efficiencies, compared to combustion based technologies. Fuel cells have been considered as the frontrunner in the search for an ideal energy source for stationary and mobile applications such as automobile, portable devices and various material handling equipment etc.[2, 3] In particular, proton exchange membrane fuel cells (PEMFCs) are considered as promising power sources due to the use of hydrogen fuel which is indeed light-weight, clean (low carbon footprint) and also bodes the advantage of low operating temperatures (<120^{o}C).[3] These unique PEMFCs features offer quick start-up, extended durability of system components including ease of operation, reduced cost and high reliability.[3] However, the difficulty to handle hydrogen gas combined with the capital costs and durability of the system are the major constraints for commercialization of PEMFCs. The capital cost of expensive platinum group metals (PGM) based electro-catalysts (e.g. Pt/C) albeit possessing excellent electrochemical activity and electrochemical stability/durability as PEMFC anode and cathode materials, is primarily considered to be responsible for impeding the large-scale commercialization of PEMFC.[2, 3, 5, 6] Hence, there is considerable demand and the much needed impetus for the development of novel non-noble metal or reduced noble metal containing

electro-catalysts exhibiting high electrochemical activity and stability/durability for PEMFCs since it will likely minimize the precious metal loading to ultra-low levels without compromising the electrochemical activity of the parent noble metal.

In the pursuit of identification and development of high performance and durable non-noble metal or reduced noble metal containing electro-catalyst, an approach that is adopted is the alloying of noble metals (e.g. Pt, Ir) with transition metals such as Fe, Sn, Ni, Mo [7-13], offering reduced noble metal content without compromising electrochemical performance and stability. For example, different platinum based binary and ternary alloys with reduced noble metal loading exhibiting superior electrochemical activity and stability have been developed. These include Pt-Sn/C and Pt-Sn-Ir/C ternary alloy for ethanol oxidation and Pt-Co, Pt(Ru)/TiN[2], Pt-Ni-Cr/C and Pt-CuO/C for methanol oxidation.[14-17] In addition, Pt-Ti/C for oxygen reduction reaction (ORR) and Pt-Ni/C, Pt-WO_3-TiO_2/C, $Co_{1-x}(Ir_x)$ (x=0.2, 0.3, 0.4)[3] for hydrogen oxidation reaction (HOR) for PEMFC are some examples of reduced noble metal containing alloys that have been reported which have demonstrated good electrochemical performance and stability.[7, 12, 18] On the other hand, non-noble metal systems, *e.g.* tungsten based catalysts has been explored in various types of fuel cells such as PEMFC, direct methanol fuel cell, direct ethanol fuel cell and molten carbonate fuel cells.[19] In particular, tungsten trioxide (WO_3) and tungsten carbide have been studied as co-catalysts and catalyst supports due to their high electrical conductivity and chemical stability/durability in acidic media.[20, 21] Tungsten trioxide has received special interest as a co-catalyst to Pt/C for HOR due to its tendency to form hydrogen tungsten bronze (H_xWO_3; $0<x<1$) attributed to the hydrogen spillover effect.[20-25] Apart from these studies of WO_3 used as co-catalyst, there are limited studies into the proper design and development of WO_3

based alloy electro-catalyst which can exhibit excellent electrochemical activity and stability for HOR as PEMFC anodes.[26]

In the present study, first-principles calculations of the total energies, electronic structures and cohesive energies have been carried out to identify a suitable WO_3 based alloy for HOR. Based on the theoretical calculations, WO_3-IrO_2 solid solutions denoted as $(W_{1-x}Ir_x)O_y$ (x=0.2, 0.3; y=2.7-2.8) of different compositions have been explored as a suitable anode electro-catalyst for HOR in PEMFC. The rationale for selection of IrO_2 is that Ir and IrO_2 have garnered interest as novel electro-catalysts for different electrochemical processes such as hydrogen oxidation reaction[3], ethanol oxidation reaction[27], oxygen reduction reaction (ORR)[28] and oxygen evolution reaction[29] during water electrolysis.[27, 29, 30] However, there are limited studies into IrO_2 based catalysts for HOR on PEMFC anodes due to the well-known instability of IrO_2 in the HOR operating conditions.[26] The incorporation of Ir into the WO_3 framework to form a solid solution offers the unique prospects of maintaining the structural and chemical integrity of WO_3, while simultaneously exploiting the excellent electrical conductivity and electrochemical activity under the stringent acidic PEMFC conditions.

In the present investigation, $(W_{1-x}Ir_x)O_y$ (x=0.2, 0.3; y=2.7-2.8) solid solution in nanoscale dimensions has been synthesized by a two-step wet chemical synthesis route. The synthesis method is very important to obtain the electro-catalyst in the nanostructured form exhibiting high electrochemical active surface area (ECSA) and thus, achieve the desired superior electrochemical activity and stability, which together will result in the much desired reduced noble metal loading. At first, WO_3 nanoparticles (WO_3-NPs) have been synthesized followed by the formation of solid solution, $(W_{1-x}Ir_x)O_y$ in the second step by suitably heat treating WO_3 and iridium precursor ($IrCl_4$) mixture in air at 673 K. The present report thus documents the

theoretical and experimental studies combined with the electrochemical performance of nanostructured $(W_{1-x}Ir_x)O_y$ (x=0.2, 0.3; y=2.7-2.8) electro-catalyst for HOR of PEMFC under the appropriate PEMFC operating conditions.

2. Computational methodology

The overall catalytic activity of the $(W_{1-x}Ir_x)O_y$ oxide electro-catalyst is expected to depend on the electronic structure as well as the long term stability of the electrode. The effect of compositions on the electronic structure, structural stability and the electro-catalytic activity of the material could be best understood from the theoretical considerations. The computational component of the present study is to investigate the electronic properties of $(W_{1-x}Ir_x)O_y$ electro-catalyst as a function of its chemical composition. The total energy, electronic and optimized crystal structures as well as total and projected densities of electronic states for $(W_{1-x}Ir_x)O_y$ solid solution have been calculated using the first principles approach within the density functional theory. For comparative purposes, pure platinum as gold standard electro-catalyst for PEM fuel cells has also been considered in the present study.

Hydrogen oxidation reaction in PEMFC occurs on the surface of the catalyst. There is a need to investigate the surface electronic and structural properties of the materials. For computational simplicity, $(W_{0.75}Ir_{0.25})O_y$ composition has been chosen for calculating the surface properties of the $(W_{1-x}Ir_x)O_y$ solid solution. Such a composition although slightly different from the experimental composition (x=0.2, 0.3) described in the experimental sections of the manuscript nevertheless allows for the selection of smaller representative super-cell for all the calculations of the electronic structures employed in the present study. The $(W_{1-x}Ir_x)O_y$ solid solutions exhibit the same crystal structure as pure WO_3 belonging to monoclinic $P2_1/c$

symmetry, space group #14, which is a perovskite-like structure with eight WO_3 formula units in the elementary unit cell which is confirmed from the experimental work.[31, 32] Thus, for the surface properties calculations, a five atomic layer two-dimensional slab with three mixed metal-oxygen layers and two pure oxygen layers in a direction perpendicular to (001) plane has been selected in this study. Accordingly, a slab ~7.5 Å in thickness containing 9 atoms of W, 3 atoms of Ir (with one Ir and three W atoms at each mixed metal-oxygen layer) and 38 atoms of O has been separated from its image perpendicular to the surface direction by a vacuum layer of ~15 Å.

The total energies, electronic structure and density of electronic states of the surface and bulk were calculated using the Vienna Ab-initio Simulation Package (VASP) within the projector-augmented wave (PAW) method [33-35] and the generalized gradient approximation [36] for the exchange-correlation energy functional in a form suggested by Perdew and Wang.[37] This program calculates the electronic structure and inter-atomic forces from quantum mechanics first principles methodologies. Standard PAW potentials were employed for the Ir, W and O potentials containing nine, six, and six valence electrons, respectively.

For all the materials considered, the plane wave cutoff energy of 520 eV has been chosen to maintain a high accuracy of the total energy calculations. The lattice parameters and internal positions of atoms were fully optimized employing the double relaxation procedure, and consequently, the minima of the total energies with respect to the lattice parameters and internal ionic positions have been determined. This geometry optimization was obtained by minimizing the Hellman–Feynman forces via a conjugate gradient method, so that the net forces applied on every ion in the lattice are close to zero. The total electronic energies were converged within 10^{-5} eV/un.cell resulting in the residual force components on each atom to be lower than 0.01 eV/Å/atom, thus allowing for an accurate determination of the internal structural parameters for

the oxide. The Monkhorst-Pack scheme was used to sample the Brillouin Zone (BZ) and generate the ***k***-point grid for all the materials considered in the present study. A choice of the appropriate number of ***k***-points in the irreducible part of the BZ was based on convergence of the total energy to 0.1 meV/atom.

3. Experimental methodology

3.1 Preparation of Electro-catalyst

Synthesis of WO_3-NPs

Sodium tungstate dihydrate ($Na_2WO_4.2H_2O$, 99%, Aldrich) was used as the tungsten precursor for the synthesis of WO_3-NPs. Specifically $Na_2WO_4.2H_2O$ was dissolved in D.I. water, purified by the Milli-Q system (18 MΩ cm deionized water, Milli-Q Academic, Millipore). The pH of the aqueous solution of $Na_2WO_4.2H_2O$ was then adjusted to ~0.5 by adding hydrochloric acid (HCl, 37%, Aldrich). This solution was then well-stirred for ~1 h and then heated to $65^oC \pm 5^oC$. The reaction temperature was maintained at $65^oC \pm 5^oC$ for ~30 min to ensure completion of the reaction. The resultant slurry was subsequently centrifuged and washed repeatedly with water purified by the Milli-Q system (18 MΩ cm deionized water, Milli-Q Academic, Millipore) followed by drying at ~50^oC for ~6 h, yielding the hydrated tungsten trioxide (H_2WO_4). To synthesize pure WO_3 nanoparticles (WO_3-NPs), the dried powder was heat-treated in ultra high-pure (UHP) argon atmosphere (Matheson; 99.99%, flow rate = $100cm^3$/min) at 623 K for 2 h, in accordance with the thermogravimetric results for H_2WO_4 conducted in UHP-Ar atmosphere (see **Section S1** and **Fig. S1** in supporting information).

Synthesis of $(W_{1-x}Ir_x)O_y$ (x=0.2, 0.3)

Tungsten iridium oxide solid solution compositions, $(W_{1-x}Ir_x)O_y$ were synthesized by soaking the as-prepared WO_3 in a stoichiometric amount of $IrCl_4$ (Aldrich). This was achieved by dissolving $IrCl_4$ in absolute ethanol inside an atmosphere controlled glove box (MBraun Unilab Work station) to prevent any undesired side reaction, followed by the addition of WO_3-NPs synthesized by the procedure mentioned above. The soaked powder was then dried in a crucible in an oven at 60^{o}C for 2 h to remove the alcohol and subsequently heat treated in air at 673 K for 4 h to form the desired $(W_{1-x}Ir_x)O_y$ (x=0.2, 0.3) solid solutions. For comparison of the electro-catalytic activity of $(W_{1-x}Ir_x)O_y$ with IrO_2, IrO_2 nanoparticles (IrO_2-NPs) were also synthesized by heat-treatment of the commercially obtained $IrCl_4$ (Aldrich) in air at 673 K for 4 h.

3.2 Electro-catalyst characterization

3.2.1 Structural characterization

X-ray diffraction

Qualitative phase analysis of $(W_{1-x}Ir_x)O_y$ electro-catalyst was carried out using X-ray diffraction (XRD). Philips XPERT PRO system was used for the XRD analysis, employing CuK_α (λ = 0.15406 nm) radiation at an operating voltage and current of 45 kV and 40 mA, respectively. The Lorentzian and Gaussian contribution from the peak was determined by peak profile analysis of $(W_{1-x}Ir_x)O_y$ using the Pseudo-Voigt function. The single line approximation method was employed for determination of the integral breadth of the Lorentzian contribution. The contribution from the instrumental broadening and lattice strain contribution was eliminated

from the integral breadth of the Lorentzian contribution and further used to calculate the particle size of the $(W_{1-x}Ir_x)O_y$, using the Scherrer formula.[2-4]

Thermal analysis

The phase formation and decomposition temperature of H_2WO_4 obtained following the reaction of $Na_2WO_4.2H_2O$ and HCl to form phase pure WO_3 (**Section S1**) was ascertained by conducting thermogravimetric analysis (TGA) using a TGA-DTA machine (Netzsch STA 09PC/4/H/Luxx TG-DTA). The TGA analysis has been carried out employing a heating rate of 10^oC/min from room temperature up to 773 K in ultra-high purity Argon (UHP-Ar) atmosphere.

Microstructure analysis

The microstructure of $(W_{1-x}Ir_x)O_y$ electro-catalyst was studied using scanning electron microscopy (SEM). Energy dispersive x-ray spectroscopy (EDAX) analyzer (attached with the SEM machine) was used for semi-quantitative elemental analysis and to ensure homogeneous distribution of elements (by x-ray mapping) without undergoing any phase segregation on a specific site. The elemental and x-ray mapping analysis was carried out using Philips XL-30FEG equipped with an EDAX detector system with an ultrathin beryllium window and Si(Li) detector operating at 20 kV. The particle size and the structure of $(W_{1-x}Ir_x)O_y$ particles was studied using transmission electron microscopy using JEOL JEM-2100F.

X-ray photoelectron spectroscopy

The oxidation states of W, Ir and O in $(W_{1-x}Ir_x)O_y$ were investigated by conducting X-ray photoelectron spectroscopy (XPS) on the electro-catalyst materials. A Physical Electronics (PHI) model 32-096 X-ray source control and a 22-040 power supply interfaced to a model 04-548 X-ray source with an Omni Focus III spherical capacitance analyzer (SCA) was used for XPS

analysis of the catalyst materials. The system was operated in the pressure range of 10^{-8} to 10^{-9} Torr (1.3×10^{-6} to 1.3×10^{-7} Pa). Calibration of the system was carried out by following the manufacturer's procedures, wherein the photoemission lines, E_b of Cu $2p_{3/2}$ (932.7 eV), E_b of Au $4f_{7/2}$ (84 eV) and E_b of Ag $3d_{5/2}$ (368.3eV) were utilized employing a magnesium anode. The experimentally determined peak areas were correspondingly divided by the instrumental sensitivity factors to determine the desired intensities and these intensity values were reported in this study. The adventitious C 1s peak to 284.8 eV was considered as a reference for the charge correction.

3.2.2 Electrochemical characterization

Electrochemical characterization of the electro-catalysts were conducted using a H_2 saturated 0.5 M sulfuric acid (H_2SO_4) solution as the electrolyte at 40°C (using a Fisher Scientific 910 Isotemp refrigerator circulator) utilizing an electrochemical workstation (VersaSTAT 3, Princeton Applied Research). Initially, the electrolyte solution, i.e., 0.5 M sulfuric acid (H_2SO_4) was purged with UHP-N_2 for complete removal of oxygen from the test cell. A three electrode configuration was used for the test cell setup. The working electrodes were prepared utilizing the catalyst ink consisting of 85 wt% catalyst and 15 wt% Nafion 117 (5 wt.% solution in lower aliphatic alcohols, Aldrich) that was spread on the teflonized carbon paper. The total catalyst loading of ~0.4 mg on 1 cm^2 area was used for the electrochemical characterization of the $(W_{1-x}Ir_x)O_y$ electro-catalyst irrespective of the compositions. A Pt wire was used as the counter electrode and mercury/mercurous sulfate (Hg/Hg_2SO_4) electrode (XR-200, Hach) (+0.65V *vs* NHE) was used as the reference electrode. The electrochemical performance of the $(W_{1-x}Ir_x)O_y$ electro-catalyst is compared with the state of the art Pt based

electro-catalyst in this study. Hence accordingly, the electrochemical characterization of commercial 40% Pt/C electro-catalyst (Alfa Aesar) was also carried out utilizing loading of ~0.4 mg of Pt on 1 cm^2 area under the same operating conditions. Also, pure WO_3-NPs and IrO_2-NPs were also tested under the same identical operating conditions utilizing similar and identical total active material loading of ~0.4 mg on 1 cm^2 electrode area.

Cyclic voltammetry/Linear sweep voltammetry

The cyclic voltammetry (CV) curves were obtained by scanning the potential between -0.092 V (*vs* NHE) and 1 V (*vs* NHE) at 10 mV/sec. Also, linear sweep voltammetry (LSV) was carried out by scanning potential between -0.05 V (*vs* NHE) to 0.4 V (*vs* NHE) at 10 mV/sec. LSV of the different electro-catalyst materials were iR_Ω corrected, where R_Ω is the ohmic resistance determined from electrochemical impedance spectroscopy (EIS) analysis described below and the current density at 0 V *vs* NHE (standard redox potential of HOR) was used to compare the electrochemical performance of all of the different electro-catalyst materials. The Tafel plot obtained after iR_Ω correction represented by the equation $\eta = a + b \log i$ (plot of overpotential, η *vs* log current, log *i*) and the corresponding Tafel slope (b) has been used to study the reaction kinetics.

Electrochemical impedance spectroscopy

Electrochemical impedance spectroscopy (EIS) was carried out to determine the ohmic resistance (R_Ω) (which includes resistance of components including electrolyte and electrode) and the charge transfer resistance (R_{ct}) of the electro-catalyst materials. The frequency range of 100 mHz-100 kHz at ~0.016 V and 10mV amplitude was employed for EIS which was executed

using the electrochemical work station (VersaSTAT 3, Princeton Applied Research). The experimentally obtained EIS plot was then fitted using the ZView software from Scribner Associates with circuit models, $R_\Omega(R_{ct}Q_1W_o)$, where Q_1 is constant phase element, representing capacitance behavior of the catalyst surface and W_o is open circuit terminus Warburg element.[2-4, 38] R_Ω was used for ohmic loss correction (iR_Ω) in the LSV curves of electro-catalyst materials and the charge transfer resistance of the synthesized electro-catalysts was determined from R_{ct}.

Reaction kinetics study

A rotating disk electrode (RDE) setup was used to conduct the polarization studies for the synthesized electro-catalysts and evaluation of the reaction kinetics of all the electro-catalysts. For these studies, the catalyst ink (85 wt% catalyst and 15 wt% Nafion 117) was sonicated and applied to a glassy carbon (GC) disk (geometric area=0.19 cm^2) followed by drying in air at room temperature. A thin layer of catalyst (1.15 mg cm^{-2}) applied on the surface of the disk was used as the working electrode. The counter electrode used was Pt wire and similar to the catalytic activity and electrochemical response studies, Hg/Hg_2SO_4 was used as the reference electrode. The polarization study was carried out in 0.5 M H_2SO_4 solution at 40^{o}C in a H_2 stream utilizing rotation speeds of 100, 400, 900, 1600 and 2500 rpm, respectively. Multiple small potential steps (see **Fig. S2**) were employed in the polarization study to minimize the charging current contribution.[3] Accordingly, the current was measured at the end of each step.[3, 39] The Koutechy-Levich equation was used to find number of electrons produced in the reaction (n) and kinetic current (i_k)[3, 39]:

$$i^{-1} = i_k^{-1} + i_L^{-1}$$

$$i_L = 0.62\, n\, F\, A_e\, D_0^{2/3}\, \omega^{1/2}\, \nu^{-1/6}\, C_o^*$$

Here, i_L is the limiting current (A), i_k is the kinetic current (A) observed in the absence of mass transfer limitations, F is Faraday constant (C/mol), A_e is the geometric area of the electrode (0.19 cm^2), D_0 is diffusivity (cm^2/sec), ω is rotation speed (rad/sec), ν is the kinematic viscosity of the electrolyte, C_o^* is the bulk concentration of H_2 in 0.5 M H_2SO_4.

Electrochemical stability/durability test

The electrochemical stability/durability of the synthesized electro-catalysts was studied by conducting chronoamperometry (CA) (current density *vs* time) for 24 h using 0.5 M H_2SO_4 as the electrolyte at 40°C at a constant voltage of ~0.016V *vs* NHE. The electrolyte (H_2SO_4) solution was accordingly collected after 24 h of CA testing of each electro-catalyst material and analyzed by inductively coupled plasma optical emission spectroscopy (ICP-OES, iCAP 6500 duo Thermo Fisher) to determine the amount of elemental tungsten and iridium leached out into the electrolyte solution from the electrode. The amount of elements leached out into the electrolyte solution will accordingly relate to the electrochemical stability/durability of the synthesized WO_3 based electro-catalysts.[2-4]

Membrane electrode assembly (MEA) preparation and single cell test analysis

The MEA for evaluation of the catalyst performance in single cell studies were prepared. For non-platinum anode, the catalyst ink was prepared consisting of 85 wt.% catalyst and 15 wt.% Nafion 117 solution (5 wt.% solution in lower aliphatic alcohols, Sigma-Aldrich). For the anode, the total loading of $(W_{0.7}Ir_{0.3})O_y$ was 0.2 mg cm^{-2}. For comparison, 40% Pt/C (Alfa Aesar) was also studied as anode electro-catalyst in single cell test using loading of 0.2 mg of Pt cm^{-2}. For the cathode, the catalyst ink was prepared using 40% Pt/C electro-catalyst (Alfa Aesar)

using the same amount as mentioned above, i.e., 85 wt.% catalyst and 15 wt.% Nafion 117 solution (5 wt.% solution in lower aliphatic alcohols, Sigma-Aldrich). Loading of 0.3 mg of Pt cm^{-2} was also used for cathode electro-catalyst. The electrodes were prepared by spreading the electro-catalyst ink on teflonized carbon paper. For the single cell testing, the membrane electrode assembly (MEA) was fabricated by using a Nafion 115 membrane which was sandwiched between the anode and cathode. The Nafion 115 membrane was pretreated first with a 3 wt.% hydrogen peroxide solution to its boiling point to oxidize any organic impurities. Subsequently, it was boiled in D.I. water followed by immersion in a boiling 0.5 M sulfuric acid solution to eliminate impurities. Finally, it was treated multiple times in D.I water to remove any traces of remnant acid. This membrane was then stored in D.I. water to avoid dehydration. The Nafion 115 membrane was sandwiched between the anode and cathode by hot-pressing using a 25T hydraulic lamination hot press with dual temperature controller (MTI Corporation) at a temperature of 125^{o}C and pressure of 40 atm applied for 30 sec to ensure good contact between the electrodes and the membrane. This MEA was then used in the single cell test analysis, which was carried out using fuel cell test set up obtained from Electrochem Incorporation at 80^{o}C and 0.1 MPa using UHP-H_2 (200 ml/min) and UHP-O_2 (300 ml/min) as the reactant gases.[3]

4. Results and discussion:

4.1 Electrochemical performance of WO_3-NPs, IrO_2-NPs and state of the art 40% Pt/C

4.1.1 Structural characterization of the WO_3-NPs and IrO_2-NPs

The possible reaction scheme based on the TGA results indicating the temperature of formation of the WO_3 nanoparticles from H_2WO_4 generated as a product in the reaction of

sodium tungstate dehydrate ($Na_2WO_4.2H_2O$) with HCl, has been discussed in the supplementary section (see **Section S1** and **Fig. S1**). The XRD pattern of the synthesized pure WO_3 NPs displayed in **Fig.1** shows the monoclinic structure as expected. The XRD pattern for pure IrO_2 (**Fig. 1**), obtained following heat treatment of $IrCl_4$ at 673 K in air also shows the expected tetragonal structure.

4.1.2 Electrochemical characterization of WO_3-NPs, IrO_2-NPs and state of the art 40% Pt/C

The CV curves of the synthesized pure WO_3 nanoparticles (WO_3-NPs), IrO_2 nanoparticles (IrO_2-NPs) and the commercially obtained Pt/C obtained in H_2-saturated 0.5 M H_2SO_4 solution at 40^{o}C are shown in **Fig. 2a**. The strong hydrogen oxidation peak at ~0 V (*vs* NHE) for Pt/C and IrO_2-NPs (**Fig. 2a**) shows the high electrochemical activity for both systems for the occurrence of HOR. On the other hand, a rather inferior current density is seen for pure WO_3-NPs at ~0 V compared to the synthesized IrO_2-NPs and commercially obtained Pt/C indicating poor activity of the synthesized WO_3-NPs for HOR. The chemically synthesized WO_3-NPs show a peak at a high potential (~0.22 V), which can be attributed to the oxidation of the tungsten bronze, H_xWO_3 phase which contributes to the additional anodic current density.[20, 22, 25] The uncorrected and iR_Ω corrected LSV curves for the HOR occurrence for WO_3-NPs, IrO_2-NPs and Pt/C are shown in **Fig. 2b**. The onset potential for the occurrence of HOR for WO_3-NPs ~(0.011 V), seen in the iR_Ω corrected LSV curve (**Fig. 2b**), is higher than that seen for Pt/C ~(-0.025V) and for the synthesized IrO_2-NPs ~(-0.018V) (also see **Table 1**). This result clearly suggests that the chemically synthesized WO_3-NPs exhibits a higher reaction polarization in the Tafel step (*i.e.* H_2 + 2M $\rightarrow$2MH, M=catalyst) for the HOR electro-catalyst reaction compared to Pt/C and the synthesized IrO_2-NPs electro-catalyst. The chemically synthesized WO_3-NPs exhibit poor

current density (~0.0 mA cm^{-2}) at 0 V (*vs* NHE) (see **Fig. 2b**) while the commercially obtained Pt/C (~0.71 mA cm^{-2}) and the synthesized IrO_2-NPs (~0.55 mA cm^{-2}) show expectedly, a significantly higher current density at 0 V (**Table 1**). The poor electrochemical activity of the chemically synthesized WO_3-NPs for the catalytic occurrence of HOR is primarily due to the ~0.036 V higher onset potential (owing to the higher reaction polarization) of the chemically synthesized and rather very much electrochemically inactive WO_3-NPs electro-catalyst with respect to the commercially obtained Pt/C (**Table 1**). Additionally, the charge transfer resistance (R_{ct}), which is related to reaction kinetics occurring on the surface of electro-catalyst and determined from EIS analysis which will be discussed in detail later for the chemically generated WO_3-NPs (~37 Ωcm^2) is almost three fold higher than that of the commercially obtained Pt/C electro-catalyst (~13 Ωcm^2) and approximately two-fold higher than the synthesized IrO_2-NPs (~16Ωcm^2) (**Table 2**). This shows the rather poor and very much inactive reaction kinetics for the hydrogen ion generating HOR and thus as a consequence, a very poor electrochemical activity of the chemically derived WO_3-NPs for HOR compared to the commercially obtained Pt/C and chemically synthesized IrO_2-NPs.

The electrochemical stability/durability of WO_3-NPs along with IrO_2-NPs and Pt/C electro-catalyst was analyzed by performing chronoamperometry (CA) study in order to further assess the electrochemical performance. The test was conducted for 24 h at the constant potential of ~0.016V (*vs* NHE) (which is closer to 0 V, standard redox potential of HOR). The CA curve of WO_3-NPs, IrO_2-NPs and Pt/C is shown in **Fig. 3**. As shown in the figure, the current density attains a steady value after 2 h for WO_3-NPs and Pt/C (**Fig. 3)**. The current density decreased from ~0.04 mA cm^{-2} after 2 h to ~0.035 mA cm^{-2} after 24 h for WO_3-NPs, indicating a loss of almost ~11% in current density. For Pt/C on the other hand, the current density degrades from

~0.65 mA cm^{-2} after 2 h to only ~0.61 mA cm^{-2} after 24 h. Thus, a loss of only ~5% in current density is seen for Pt/C at the end of the CA test. However, a drastic decrease in current density (from ~0.29 mA cm^{-2} after 2 h to ~0.11 mA cm^{-2} after 24 h, 62% loss) has been noted for the chemically synthesized IrO_2-NPs due to the instability of IrO_2 under the hydrogen oxidation reaction conditions.[40] Hence the above results clearly show that despite the poor current density and also an inferior electrochemical activity displayed by the chemically synthesized WO_3-NPs for HOR at 0 V (*vs* NHE), the system nevertheless demonstrates excellent electrochemical stability with minimal loss in catalytic activity.

4.2 Computational study for predicting the solid solution $(W_{1-x}Ir_x)O_y$ compositions exhibiting high electrochemical activity

The experimental results discussed so far clearly show that the chemically synthesized WO_3-NPs though active for HOR, however exhibit poor electrochemical activity due to the high reaction polarization. However as discussed above, chemically synthesized WO_3-NPs display impressive electrochemical stability following the chronoamperometry test conducted for HOR in the electrolyte solution (0.5 M H_2SO_4). These results thus clearly suggest that WO_3 based system would be an excellent choice as an electro-catalyst for HOR if the polarization resistance could be reduced to a significant level comparable to that of the commercially obtained Pt/C exhibiting excellent electrochemical activity. On the other hand, IrO_2-NPs do display excellent electrochemical activity with low reaction polarization for HOR. However, it shows poor electrochemical stability in the electrolyte solution. Hence, in order to improve the catalytic activity of WO_3 based system by reducing the polarization resistance, a WO_3 based catalyst with IrO_2 as solute (solid solution of IrO_2 and WO_3), denoted as $(W_{1-x}Ir_x)O_y$ is explored in the current work as a possible potential electro-catalyst for HOR in PEMFC. In addition, the $(W_{1-x}Ir_x)O_y$

428 solid solution is expected to show excellent durability since all the solid solution compositions
429 exhibit the preferred WO_3 crystal structure, as reported in the experimental section. Theoretical
430 first principles electronic structure calculations have thus been carried out to identify suitable
431 electro-catalyst composition of $(W_{1-x}Ir_x)O_y$, with unique electronic structure, which can exhibit
432 excellent electrochemical activity and durability for HOR.

433 The catalytic activity and thus the total polarization of a chemical reaction can be
434 qualitatively understood by conducting numerical analysis of the electronic structure of the
435 catalyst materials. This approach is based on the inspiring concept proposed by J.K. Nørskov *et.*
436 *al.* [41, 42] regarding the existence of a simple descriptor for determining the catalytic activity of the
437 surface. This descriptor has been defined by the gravity center of the transition metal d-band ε_d
438 usually located in the vicinity of the Fermi level. An optimal position of the d-band center thus
439 provides a highly favorable interaction between the catalytic surface and the various species
440 participating in the catalytic reactions predominantly occurring on the surface leading to the
441 maximum expected catalytic activity. Such an interaction should thus be considered optimal,
442 leading to a moderate effect allowing the reagents and products to both adsorb on the surface and
443 also desorb most efficiently from the same. Hence an adjustment of the d-band center position
444 with respect to the Fermi level may likely play a critical role contributing to the design of novel
445 highly active and electrochemically stable electro-catalysts discussed herein.

446 **Fig. 4** shows the projected d-band densities of states (DOS) together with the
447 corresponding d-band center (ε_d) of these zones marked with vertical arrows on the graphs
448 calculated for *fcc* (111) crystallographic orientation of pure Pt. Since pure Pt is considered as a
449 gold standard for PEMFC electro-catalyst, the d-band position for Pt could serve as a reference
450 point (or a benchmark) for the optimal catalytic activity of the designed materials. In **Fig. 4a**, it

can be seen that the d-band center (ε_d) of pure Pt is located below the Fermi level at ~(-1.33 eV). It is also expected that IrO_2 will exhibit similar electro-catalytic activity due to ε_d (-1.33 eV) similar to that of Pt.[30] Thus, it is expected that an optimal highly favorable interaction between the catalytic surface and the various species participating in the catalytic reactions predominantly occurring on the IrO_2 surface will be similar to Pt.

In the aim of finding the electro-catalyst with minimum onset potential and improved reaction kinetics for HOR occurrence compared to Pt/C, solid solutions of WO_3 and IrO_2, denoted as $(W_{1-x}Ir_x)O_y$ have been studied as a suitable electro-catalysts for HOR in this study. In the present work, the electronic structure of the (001) surface with $(W_{0.75}Ir_{0.25})O_y$ composition has been calculated and the positions of the corresponding d-band centers have been obtained as a first moment of $n_d(E)$: $\varepsilon_d = \int n_d(E)E\mathrm{d}E / \int n_d(E)\mathrm{d}E$, where $n_d(E)$ is the projected d-band density of states of the corresponding materials. **Fig. 4** shows projected d-band densities of states together with corresponding ε_d centers of these zones marked with vertical arrows on the graphs calculated for the total and partial d-Ir and d-W components of $(W_{0.75}Ir_{0.25})O_y$ model compound with (001) orientation of the surface. The closer the corresponding d-band center to the pure Pt d-band center position, the better is the expected overall catalytic activity of the studied material. Such an approach can thus help clarify a dependence of the electro-catalytic activity of $(W,Ir)O_y$ oxide on its chemical composition.

Following the above study, **Fig. 4b** demonstrates the projected density of d-electronic states calculated for $(W_{0.75}Ir_{0.25})O_y$ composition. From this graph it can be seen that the d-band center for the combined d-bands of Ir and W is located at -1.14 eV, which is higher on the energy scale than the ideal position belonging to pure Pt (-1.33 eV). Hence, $(W_{0.75}Ir_{0.25})O_y$ is likely to exhibit lower catalytic activity than Pt and also, the optimal composition of the oxide which is

desired to exhibit d-band center similar to Pt. **Fig. 4c** and **Fig. 4d** demonstrate the projected d-Ir and d-W components of the densities of electronic states for $(W_{0.75}Ir_{0.25})O_y$. Consideration of these components may help determine the optimal chemical composition of the $(W_{1-x}Ir_x)O_y$ oxide characterized by d-band center position located exactly at -1.33 eV (the same as that of Pt). For these purposes, the d-band centers of the projected component d-Ir and d-W bands are assumed to be fixed at the present positions (-3.81 eV and -0.25 eV, respectively) and thus, independent of the chemical composition of the oxide within a relatively narrow composition range (ca. $0.15<x<0.35$). Only, the total number of d-electrons and corresponding projected d-Ir and d-W components of the density of states values are assumed to be dependent on the chemical composition of the oxide. In such a situation, the optimal composition x could be derived from the following equation relating the d-band center to the composition:

$$\varepsilon_d[(W_{1-x}Ir_x)O_3] = (1-x)\,\varepsilon_d[\text{d-W}] + x\varepsilon_d[\text{d-Ir}],$$

where, $\varepsilon_d[(W_{1-x}Ir_x)O_3] = -1.33$ eV; $\varepsilon_d[\text{d-Ir}] = -3.81$eV; and $\varepsilon_d[\text{d-W}] = -0.25$ eV.

Solution of this equation provides a value for the optimal composition, x = 0.303. Hence, 70 at.% W and 30 at.% Ir, .i.e., $(W_{0.7}Ir_{0.3})O_y$ composition is selected for further experimental studies. It should also be noted that a further increase of the Ir content (beyond x=0.3) will result in a gradual movement of the overall Ir5d-W5d-band center downward on the energy scale deteriorating the expected electro-catalytic activity of the solid solution. Of course, this highly qualitative consideration does not apply on a whole range of Ir-compositions and is constrained only by quite a narrow concentration interval centered about the directly calculated $(W_{0.75}Ir_{0.25})O_y$ compound, as discussed earlier. Compositions laying outside of this range could be considered by direct calculations of the electronic structure of the material characterized by its

own specific crystal structure obtained from the experimental data and which could be different from that of $(W_{0.75}Ir_{0.25})O_y$ used in the present study.

4.3 Synthesis and characterization of theoretically predicted $(W_{1-x}Ir_x)O_y$ alloy compositions

4.3.1 Structural characterization of $(W_{1-x}Ir_x)O_y$

Solid solution of WO_3 and IrO_2,.i.e., $(W_{1-x}Ir_x)O_y$ of different compositions (x=0.2, 0.3) were synthesized by a two-step chemical approach as discussed in the experimental methodology above in order to verify the theoretically determined results discussed above by experiments. The XRD patterns the $(W_{1-x}Ir_x)O_y$ (x=0.2, 0.3), shown in **Fig. 1**, display the compositions to have the monoclinic structure similar to WO_3. No XRD peaks corresponding to presence of any tetragonal IrO_2 have been detected, which indicates the complete dissolution of IrO_2 into the WO_3 parent structure leading to the formation of solid solution of IrO_2 and WO_3 with monoclinic phase. The particle size of $(W_{0.7}Ir_{0.3})O_y$, calculated using the Scherrer's formula, is ~8 nm, confirming the formation of nanoparticles of the solid solution. The TEM bright field image of $(W_{0.7}Ir_{0.3})O_y$, shown in **Fig. 5**, shows nanometer sized particles in the range ~7-10 nm, which is in good agreement with the XRD analysis.

The SEM image and elemental x-ray mapping along with EDAX pattern of a representative composition $(W_{0.7}Ir_{0.3})O_y$, is shown in **Fig. 6 (a-b)**. The presence of W and Ir is confirmed from EDAX pattern of $(W_{0.7}Ir_{0.3})O_y$ (**Fig. 6b**). Semi-quantitative elemental composition analysis of $(W_{0.7}Ir_{0.3})O_y$ electro-catalyst was obtained by EDAX, which showed the measured elemental compositions of W and Ir to be close to the nominal composition (**Fig. 6b**). Also, it should be noted there is no segregation of W, Ir and O seen in the particles of

$(W_{0.7}Ir_{0.3})O_y$, as evidenced in the elemental x-ray maps of W, Ir and O (**Fig. 6a**) confirming homogeneous distribution of the individual elements within the chemically synthesized particles.

The chemical oxidation states of W, Ir and O were determined using x-ray photoelectron spectroscopy (XPS) analysis performed on WO_3-NPs, IrO_2-NPs and $(W_{0.7}Ir_{0.3})O_y$. The Ir 4f doublet peaks for IrO_2, observed at ~61.7 eV and ~64.5 eV (**Fig. 7a**), correspond to Ir $4f_{7/2}$ and Ir $4f_{5/2}$ binding energy, respectively that is consistent with bulk IrO_2.[43] As shown in **Fig. 7a**, Ir $4f_{7/2}$ and Ir $4f_{5/2}$ peaks of $(W_{0.7}Ir_{0.3})O_y$ catalyst are shifted to lower binding energy values by ~0.6 and ~0.4 eV, in comparison to IrO_2 catalyst. On the other hand, the W 4f doublet peaks for WO_3, observed at ~35.7 eV and ~37.9 eV (**Fig. 7b**), correspond to W $4f_{7/2}$ and W $4f_{5/2}$ binding energy, respectively consistent with bulk WO_3.[44, 45] For $(W_{0.7}Ir_{0.3})O_y$, W $4f_{7/2}$ and W $4f_{5/2}$ peaks are shifted to lower binding energy values by ~0.2 eV, compared to WO_3 (**Fig. 7b**). The shift in binding energy for both Ir-4f and W-4f doublet peaks indicate modification in the electronic structure of Ir and W by the formation of $(W_{0.7}Ir_{0.3})O_y$ solid solution. The modification of electronic structure of $(W_{0.7}Ir_{0.3})O_y$ can enhance the catalytic activity of $(W_{0.7}Ir_{0.3})O_y$ in comparison to pure WO_3-NPs and IrO_2-NPs.[2, 3] O 1s peak of pure IrO_2-NPs and WO_3-NPs is centered at ~530.4 eV and ~530.5 eV, respectively (**Fig. 7c**), which is consistent with bulk IrO_2 and WO_3.[46, 47] The O 1s peak of $(W_{0.7}Ir_{0.3})O_y$, centered at ~529.85 eV, is shifted to lower binding energy in comparison to pure WO_3 and IrO_2. The negative shift in O 1s peak for $(W_{0.7}Ir_{0.3})O_y$ can be attributed to modification of the electronic structure as a result of formation of $(W_{0.7}Ir_{0.3})O_y$ solid solution combined with accompanied possible change in density of oxygen vacancies accompanying the parent oxide. The value of y can be calculated, which is 2.7 for $(W_{0.7}Ir_{0.3})O_y$ which possibly indicates the presence of oxygen vacancies in the WO_3 parent structure. It is

expected that the presence of oxygen vacancies further modifies the structure contributing to the favorable electrochemical response for $(W_{0.7}Ir_{0.3})O_y$.[4, 48]

4.3.2 Electrochemical characterization of $(W_{1-x}Ir_x)O_y$

The electrochemical activity of $(W_{1-x}Ir_x)O_y$ (x=0.2, 0.3) as an anode electro-catalyst for PEMFCs has been studied using cyclic voltammetry. The CVs of $(W_{1-x}Ir_x)O_y$ in H_2 saturated 0.5M H_2SO_4 over a voltage window of -0.092 V and 1 V are shown in **Fig. 8a**. The CV curves show enhancement in current density at 0 V for solid solution electro-catalyst, $(W_{1-x}Ir_x)O_y$, compared to pure WO_3, which indicates improved reaction kinetics for the $(W_{1-x}Ir_x)O_y$ compositions studied. The LSV plots of HOR in H_2 saturated 0.5M H_2SO_4 of WO_3 and $(W_{1-x}Ir_x)O_y$ of different compositions and Pt/C, before and after iR_Ω correction, are shown in **Fig. 8b**. The ohmic resistance (R_Ω) for all the electro-catalyst materials was determined from the EIS Nyquist plots, as discussed later. As shown in **Fig. 8b** and plotted in **Fig. 8c**, the onset potential of $(W_{1-x}Ir_x)O_y$ for HOR shifts to lower value with increase in iridium content (**Table 1**). The lowest onset potential of [~(-0.043V *vs* NHE)] is seen for $(W_{0.7}Ir_{0.3})O_y$ (**Table 1**). It is noteworthy that the onset potentials of HOR for both (x=0.2) and (x=0.3) compositions of $(W_{1-x}Ir_x)O_y$ are [~(-0.027V *vs* NHE)] and [~(-0.043V *vs* NHE)], respectively which is lower than that of Pt/C electro-catalyst [~(-0.025V *vs* NHE)] and also, significantly lower than that of pure WO_3-NPs [(~0.011V *vs* NHE)] and pure IrO_2-NPs [(~-0.018V *vs* NHE)] (**Table 1**). This results clearly suggests that the reaction polarization of $(W_{1-x}Ir_x)O_y$ solid solution is significantly reduced due to the introduction and alloying of IrO_2 into the lattice WO_3 lattice. Hence, higher catalytic activity is expected for $(W_{1-x}Ir_x)O_y$ (x=0.2, 0.3), in comparison to IrO_2-NPs and Pt/C.

The electrochemical activity of $(W_{1-x}Ir_x)O_y$ for HOR is studied by comparing the current density at 0 V in iR_Ω corrected linear sweep voltammograms, as shown in **Fig. 8b**. Since 0 V is the standard redox potential of HOR, it is important for the electro-catalysts to exhibit high current density at 0 V with minimum overpotential.[3] Values of current density at 0 V of $(W_{1-x}Ir_x)O_y$, IrO_2-NPs and Pt/C are plotted in **Fig. 8c** and given in **Table 1**. As shown in **Fig. 8c**, $(W_{0.7}Ir_{0.3})O_y$ exhibits current density of ~0.73 mA cm^{-2} which is ~33% higher than pure IrO_2 (~0.55 mA cm^{-2}) and comparable with state of the art Pt/C catalyst (~0.71 mA cm^{-2}). On the other hand, $(W_{0.8}Ir_{0.2})O_y$ exhibits a current density ~0.42 mA cm^{-2}, which is ~77% and ~59% of IrO_2 and Pt/C, respectively. The current density of $(W_{0.7}Ir_{0.3})O_y$ at 0 V is ~74% higher than $(W_{0.8}Ir_{0.2})O_y$, which suggests a much faster reaction kinetics on $(W_{0.7}Ir_{0.3})O_y$ than $(W_{0.8}Ir_{0.2})O_y$. Additionally, this can be attributed to the lower onset potential of $(W_{0.7}Ir_{0.3})O_y$ [~(-0.043mV *vs* NHE)] than that of $(W_{0.8}Ir_{0.2})O_y$ [~(-0.027mV *vs* NHE)]. Thus, the higher electrochemical activity of $(W_{0.7}Ir_{0.3})O_y$ for HOR observed correlates very well with the first principles ab-initio studies discussed earlier.

The Tafel slope of $(W_{1-x}Ir_x)O_y$ (x = 0.2, 0.3), calculated from the iR_Ω corrected Tafel plots, are 71 and 66 mV/dec, respectively, as shown in **Fig. S3** and **Fig. S4** in the supporting section respectively (**Table 2**). The decrease in Tafel slope with increasing Ir content up to $(W_{0.7}Ir_{0.3})O_y$ suggests increase in number of electrons produced in HOR and thus, improved catalytic activity with increase in iridium content.[2, 3] Also, the Tafel slope of $(W_{0.7}Ir_{0.3})O_y$ (66 mV/dec) is lower than that of IrO_2 (69 mV/dec, **Fig. S5**) and comparable to Pt/C (67.2 mV/dec, **Fig. S6**), suggesting the excellent reaction kinetics of HOR for $(W_{0.7}Ir_{0.3})O_y$ (**Table 2**).[2, 3] The above results clearly show that $(W_{0.7}Ir_{0.3})O_y$ is indeed a promising electro-catalyst for anode of PEMFC

due to its lower polarization reflected as an observed improvement in electrochemical reaction kinetics.

Electrochemical Impedance spectroscopy

Electrochemical impedance spectroscopy (EIS) was performed at a potential of ~0.016 V over the frequency range of 100 mHz-100 kHz at an amplitude of 10mV to better understand the reaction kinetics of hydrogen oxidation on $(W_{1-x}Ir_x)O_y$ and to derive fundamental charge-transfer parameters. EIS study has also been used to determine the ohmic resistance (R_Ω) for the iR_Ω-corrected LSV curves of the electro-catalyst materials. A well-formed semicircular arc displayed in **Fig. 9** is observed at high frequencies in the EIS plot for all the electro-catalyst materials indicating a conventional one-electrochemical step charge-transfer mechanism. The diameter of this arc is typically a measure of the charge transfer resistance (R_{ct}).[2-4] The R_Ω and R_{ct} values for the electro-catalysts, obtained from fitting with a circuit model $R_\Omega(R_{ct}Q_1W_o)$, are tabulated in **Table 2**. As shown in **Table 2**, R_{ct} decreases with increase in iridium content suggesting enhancement in charge-transfer kinetics for HOR with increase in iridium content. The R_{ct} of $(W_{0.7}Ir_{0.3})O_y$ (~12 Ωcm^2) is lower than IrO_2 (~16 Ωcm^2) and similar to Pt/C (~13Ωcm^2). Also the R_{ct} of $(W_{0.7}Ir_{0.3})O_y$ is almost two-fold and three-fold lower than $(W_{0.8}Ir_{0.2})O_y$ (~30 Ωcm^2) and WO_3-NPs (~37 Ωcm^2), respectively. This explains the much improved kinetic response of $(W_{0.7}Ir_{0.3})O_y$ observed and experimentally determined in comparison to $(W_{0.8}Ir_{0.2})O_y$ and WO_3-NPs (**Table 2**), resulting in the superior electrochemical activity of HOR due to enhancement in charge transfer kinetics.

Rotating disk electrode:

Polarization studies were performed using a rotating disk electrode (RDE) setup to further study the kinetics of the electrochemical reaction and derive fundamental kinetic parameters. The current at 0 V (*vs* NHE) is used in the Koutechy-Levich equation to calculate 'n' for all the tested catalyst materials. The kinetic current (i_k), which is the current obtained in the absence of mass transfer limitations[3] is determined from the intercept on the y-axis of the Koutechy-Levich plot. Linear scan voltammograms of $(W_{0.7}Ir_{0.3})O_y$ for ω = 100, 400, 900, 1600 and 2500 rpm are shown in **Fig. 10**. The Koutechy-Levich plot of $(W_{0.7}Ir_{0.3})O_y$ is shown in the inset of **Fig. 10**. The values of n and i_k, calculated from the slope and y-axis intercept of the graph of i^{-1} versus $\omega^{-1/2}$, for $(W_{0.7}Ir_{0.3})O_y$ and Pt/C are given in **Table 3**. The value of 'n' for all the catalyst materials studied is close to the theoretical value, i.e. 2, which points to a reaction proceeding through a two electron pathway near 0 V. The linear scan voltammograms and Koutechy-Levich plot of Pt/C, for ω = 100, 400, 900, 1600 and 2500 rpm are shown in supporting information (**Fig. S7**). $(W_{0.7}Ir_{0.3})O_y$ exhibits i_k (~3.71 mA cm^{-2}), which is comparable to Pt/C (~3.41 mA cm^{-2}). This indicates that the $(W_{0.7}Ir_{0.3})O_y$ exhibits an inherent catalytic activity, similar to Pt/C. This is in accordance with the results from the EIS measurements which shows similar R_{ct} values for $(W_{0.7}Ir_{0.3})O_y$ and Pt/C (**Fig. 9** and **Table 2**). This suggests that the solid solution composition of $(W_{0.7}Ir_{0.3})O_y$ probably exhibits electronic structure similar to that of Pt as evidenced from the first principles studies of the d-band center calculations (**Fig. 4**) thus reflecting similar electro-catalytic activity as well.

The above experimental results are in good agreement with theoretical predictions (**Fig. 4**) and in addition, reflect that the optimal catalytic activity for the system might be expected for the solid solution $(W_{1-x}Ir_x)O_y$ with x~ 0.3 since the corresponding d-band center for this composition

is located at the same position on the energy scale as that of pure Pt benchmark line. It should be noted that the d-band center concept is only a *qualitative* descriptor of the surface reactivity and does not provide an absolute value of the catalytic activity. It only points to the fact that the interatomic interactions between the catalytic surface and different intermediate species involved in the hydrogen oxidation process could likely become the most optimal for $(W_{0.7}Ir_{0.3})O_y$ composition due to an appropriate changes of the electronic structure (in particular, the electronic d-band structure) during solid solution of IrO_2 and WO_3. Thus, the catalytic activity of this oxide is expected to be the highest among other chemical compositions for the $(W_{1-x}Ir_x)O_y$ system studied within a reasonable concentration range, which is indeed observed experimentally. All the experimental studies indicate that the electron transfer kinetics are facile on the surface of $(W_{0.7}Ir_{0.3})O_y$ in addition to displaying the optimal expected surface binding properties as predicted by the ab-initio studies discussed earlier. Detailed atomistic consideration of all the elementary reaction steps occurring at the surface during hydrogen oxidation reaction could shed further light on the origin of noticeable difference between electro-catalytic activities of $(W_{0.7}Ir_{0.3})O_y$ and undoped WO_3. Such a comprehensive study is not the scope of the current work and will be a subject of future computational studies that will be executed at a later point. Thus, the theoretical and experimental studies conducted herein show that $(W_{0.7}Ir_{0.3})O_y$ is indeed a promising electro-catalyst for HOR for anode of PEMFC and can be considered in the vein of the overall objective to completely replace Pt with a non-noble metal based high performance, highly durable and economically affordable electro-catalyst, a subject of considerable research interest to the entire materials and electrochemical science and technology community.

Electrochemical stability/durability test

As shown and discussed above, in addition to the inherently facile electrochemical kinetics, the electro-catalyst stability is of paramount importance. In the present study, the cohesive energies of pure Pt, and $(W_{0.75}Ir_{0.25})O_y$ have been calculated, and used as a qualitative descriptor of the chemical and structural stability of the electro-catalyst materials. The corresponding values for these materials are -5.95 eV/at, and -23.09 eV/f.un., respectively. The cohesive energies per atom would be as follows: -5.95 eV/at, and -5.77 eV/at. Of course a comparison of the cohesive energies per atom is likely to be incorrect to some extent, although it could provide some qualitative considerations towards the chemical and structural stabilities of the compared materials. Thus, one can see that pure Pt and $(W_{0.75}Ir_{0.25})O_y$ could demonstrate comparable stability. To verify these theoretical predictions experimentally, electrochemical test of the $(W_{0.7}Ir_{0.3})O_y$ composition was performed for 24 h. This was studied by carrying out chronoamperometry (CA) for 24 h at a constant potential of ~0.016V (*vs* NHE), which is closer to the standard redox potential of HOR. The CA curve of $(W_{0.7}Ir_{0.3})O_y$ is shown in **Fig. 11a**, along with that of commercially obtained Pt/C tested under identical conditions. The current density as noted becomes steady after ~2 h of initial testing for $(W_{0.7}Ir_{0.3})O_y$. A loss in activity (current density) of ~5% is observed for $(W_{0.7}Ir_{0.3})O_y$ after 24 h of testing, which is comparable with Pt/C electro-catalyst. For $(W_{0.7}Ir_{0.3})O_y$, the current density drops from ~0.72 mA cm^{-2} (after 2 h) to ~0.68 mA cm^{-2} (after 24 h), whereas the current density for Pt/C shows a current density ~0.65 mA cm^{-2} after 2 h and ~0.61 mA cm^{-2} after 24 h showing the remarkably identical electrochemical stability for the two systems.

The ICP analysis of the electrolyte solution collected after 24 h of electrochemical testing of $(W_{0.7}Ir_{0.3})O_y$ shows no presence of Ir indicating that no Ir is leached out the from electro-catalyst during the entire duration of the chronoamperometric test, whereas only a minimal

amount (~0.01 ppm) of W was present in the electrolyte solution. The CV curves of HOR on $(W_{0.7}Ir_{0.3})O_y$ and Pt/C obtained after 24 h of CA testing displayed in **Fig. 11b** also show minimal loss in catalytic activity for HOR in comparison to freshly prepared electro-catalyst. These results thus demonstrate the excellent electrochemical stability/durability of $(W_{0.7}Ir_{0.3})O_y$ that is almost comparable and similar to Pt/C.

Single cell analysis

The polarization curves of single PEMFC with $(W_{0.7}Ir_{0.3})O_y$ (total loading=0.2 mg cm^{-2}) and Pt/C (0.2 mg of Pt cm^{-2}) as anode electro-catalyst and Pt/C as cathode electro-catalyst (0.3 mg of Pt cm^{-2}) are shown in **Fig. 12 (a-b)**. Though the open circuit potential is same (0.97 V) for $(W_{0.7}Ir_{0.3})O_y$ and Pt/C, superior electrochemical activity is obtained for the $(W_{0.7}Ir_{0.3})O_y$ catalyst system similar to that of Pt/C. The maximum power density obtained using the single PEMFC with $(W_{0.7}Ir_{0.3})O_y$ as anode electro-catalyst is ~990 mW cm^{-2}, which is similar to that obtained using Pt/C as anode electro-catalyst (~990 mW cm^{-2}), respectively. The similar electrochemical activity of $(W_{0.7}Ir_{0.3})O_y$ to that of Pt/C is in accordance with the results of first principles study discussed earlier. The polarization curves of single PEMFC using $(W_{0.7}Ir_{0.3})O_y$ and Pt/C as anode electro-catalyst and Pt/C as cathode electro-catalyst after 24 h of continuous operation are also shown in **Fig. 12 (a-b)**. It should be noted that negligible loss in power density is observed for $(W_{0.7}Ir_{0.3})O_y$ and Pt/C, suggesting excellent electrochemical stability of $(W_{0.7}Ir_{0.3})O_y$, similar to that of Pt/C. These results thus suggest that $(W_{0.7}Ir_{0.3})O_y$ is indeed a promising anode electro-catalyst likely serving as a potential candidate for replacement of Pt/C in PEMFCs.

The present study hence conducted clearly demonstrates that $(W_{0.7}Ir_{0.3})O_y$ is a potential candidate for replacement of Pt/C for the hydrogen oxidation reaction (HOR) under PEMFC conditions due to its superior electrochemical performance and comparable stability/durability

with an almost 70% reduction in noble metal content. The study and the results obtained herein are thus very important and serve as a testimonial towards the realization of the long term goal to identify and determine alternative electro-catalyst systems with reduced noble metal content possessing excellent electrochemical activity and stability to replace Pt/C catalyst for commercial PEMFC systems in the near and long term future.

Conclusions

The present study shows chemically synthesized nanostructured solid solutions of $(W_{1-x}Ir_x)O_y$ with x=0.2, 0.3 and y = 2.7, 2.8 as a potential anode electro-catalyst for PEMFCs. Single phase solid solution with monoclinic structure of $(W_{1-x}Ir_x)O_y$ (x=0.2, 0.3) is observed in the XRD patterns collected on the synthesized electro-catalysts. The oxidation states of W and Ir are +6 and +4, respectively, determined from XPS analysis of $(W_{0.7}Ir_{0.3})O_y$. The value of y for $(W_{0.7}Ir_{0.3})O_y$ was determined to be 2.7 indicating modification of the electronic structure due to a possible change in density of oxygen vacancies in the solid solution, leading to superior electrochemical activity. The electrochemical performance and stability/durability of $(W_{0.7}Ir_{0.3})O_y$ is similar to that of Pt/C, as studied in half-cell configuration and single PEMFC, which is in accordance with theoretical results. Theoretical first principles electronic structure calculations reveal a strong interplay between the d-band center positions and observed overall catalytic activity of the $(W_{1-x}Ir_x)O_y$. The excellent electrochemical activity of $(W_{0.7}Ir_{0.3})O_y$ for HOR thus can be attributed to its unique composition and electronic structure, as demonstrated by the computational study. Hence, the present study demonstrates that the solid solution composition of $(W_{0.7}Ir_{0.3})O_y$ could be considered a potential candidate for replacement of Pt/C due to its superior electrochemical performance and stability/durability, which is important for

719 the development of non-noble metal based electro-catalyst with excellent electrochemical
720 activity and stability to replace Pt/C catalyst for PEMFCs.

721 **Acknowledgments**

722 Research supported by the U.S. Department of Energy, Office of Basic Energy Sciences,
723 Division of Materials Sciences and Engineering under Award DE-SC0001531 as well as in part
724 by the National Science Foundation, (Grant CBET-0933141). PNK acknowledges the Edward R.
725 Weidlein Chair Professorship funds and the Center for Complex Engineered Multifunctional
726 Materials (CCEMM) for procuring the electrochemical equipment and facilities used in this
727 research work.

728

729 **Author contributions**

730 P.P.P. and P.N.K. devised the original concept. P.P.P. designed the experiments,
731 synthesized the materials, prepared the electrodes, performed the electrochemical
732 characterization and analyzed electrochemical data. O.I.V. conducted the theoretical analyses.
733 J.P. and A.M. collected and analyzed the XPS data. P.P.P. and D. H. performed SEM and TEM
734 analyses, respectively. M.K.D. and P.J made important suggestions in the context of fundamental
735 structural and electrochemical characterization. P. P. P., P. J., M.K.D., O.I.V. and P.N.K. wrote
736 the first draft of the paper; and all authors participated in the manuscript revision. The project is
737 conceived and supervised by P.N.K.

738

739 **Supporting information**

740 TGA plot of H_2WO_4, Multuiple small potential steps used in RDE, Tafel plots of electro-
741 catalysts, RDE plot of Pt/C.

References

1. J. R. Miller, *Science*, 2012, 335, 1312-1313.
2. P. P. Patel, M. K. Datta, P. H. Jampani, D. Hong, J. A. Poston, A. Manivannan and P. N. Kumta, *Journal of Power Sources*, 2015, 293, 437-446.
3. P. P. Patel, M. K. Datta, O. I. Velikokhatnyi, P. Jampani, D. Hong, J. A. Poston, A. Manivannan and P. N. Kumta, *Journal of Materials Chemistry A*, 2015, 3, 14015-14032.
4. P. P. Patel, P. Jampani, O. Velikhokhatnyi, M. K. Datta, D. H. Hong, B. Gattu, J. A. Poston, A. Manivanan and P. N. Kumta, *Journal of Materials Chemistry A (In press)*, 2015.
5. M. Oezaslan, F. Hasché and P. Strasser, *The Journal of Physical Chemistry Letters*, 2013, 4, 3273-3291.
6. J. Chen, Y. Li, Z. Gao, G. Wang, J. Tian, C. Jiang, S. Zhu and R. Wang, *Electrochemistry Communications*, DOI: http://dx.doi.org/10.1016/j.elecom.2013.10.001.
7. F. Silva, V. Dalmazzo, M. Becker, M. Souza, R. Souza and E. A. Martini, *Ionics*, 2013, DOI: 10.1007/s11581-013-0977-z, 1-8.
8. L. G. S. Pereira, V. A. Paganin and E. A. Ticianelli, *Electrochimica Acta*, 2009, 54, 1992-1998.
9. Y. Dai, Y. Liu and S. Chen, *Electrochimica Acta*, 2013, 89, 744-748.
10. M. Götz and H. Wendt, *Electrochimica Acta*, 1998, 43, 3637-3644.
11. J. E. Hu, Z. Liu, B. W. Eichhorn and G. S. Jackson, *International Journal of Hydrogen Energy*, 2012, 37, 11268-11275.

12. M. Nagarajan, G. Paruthimal kalaignan and G. A. Pathanjali, *International Journal of Hydrogen Energy*, 2011, 36, 14829-14837.

13. D. Ham, S. Han, C. Pak, S. Ji, S.-A. Jin, H. Chang and J. Lee, *Top Catal*, 2012, 55, 922-930.

14. J. Tayal, B. Rawat and S. Basu, *International Journal of Hydrogen Energy*, 2011, 36, 14884-14897.

15. J. Xu, X. Liu, Y. Chen, Y. Zhou, T. Lu and Y. Tang, *Journal of Materials Chemistry*, 2012, 22, 23659-23667.

16. M. K. Jeon and P. J. McGinn, *Journal of Power Sources*, 2009, 188, 427-432.

17. R. S. Amin, R. M. Abdel Hameed, K. M. El-Khatib, H. El-Abd and E. R. Souaya, *International Journal of Hydrogen Energy*, 2012, 37, 18870-18881.

18. M. K. Jeon and P. J. McGinn, *Journal of Power Sources*, 2010, 195, 2664-2668.

19. E. Antolini and E. R. Gonzalez, *Applied Catalysis B: Environmental*, 2010, 96, 245-266.

20. K. Kwon, S.-a. Jin, K. H. Lee, D. J. You and C. Pak, *Catalysis Today*, DOI: http://dx.doi.org/10.1016/j.cattod.2013.12.014.

21. X. Cui, H. Zhang, X. Dong, H. Chen, L. Zhang, L. Guo and J. Shi, *Journal of Materials Chemistry*, 2008, 18, 3575-3580.

22. N. P. Lebedeva, V. Rosca and G. J. M. Janssen, *Electrochimica Acta*, 2010, 55, 7659-7668.

23. A. J. Martín, A. M. Chaparro and L. Daza, *Journal of Power Sources*, 2011, 196, 4187-4192.

24. F. Micoud, F. Maillard, A. Gourgaud and M. Chatenet, *Electrochemistry Communications*, 2009, 11, 651-654.

25. A. C. C. Tseung and K. Y. Chen, *Catalysis Today*, 1997, 38, 439-443.
26. B. Li, D. C. Higgins, D. Yang, R. Lin, Z. Yu and J. Ma, *International Journal of Hydrogen Energy*, 2012, 37, 18843-18850.
27. L. Cao, G. Sun, H. Li and Q. Xin, *Electrochemistry Communications*, 2007, 9, 2541-2546.
28. D. Yang, B. Li, H. Zhang and J. Ma, *International Journal of Hydrogen Energy*, 2012, 37, 2447-2454.
29. K. Kadakia, M. K. Datta, P. H. Jampani, S. K. Park and P. N. Kumta, *Journal of Power Sources*, 2013, 222, 313-317.
30. M. K. Datta, K. Kadakia, O. I. Velikokhatnyi, P. H. Jampani, S. J. Chung, J. A. Poston, A. Manivannan and P. N. Kumta, *Journal of Materials Chemistry A*, 2013, 1, 4026-4037.
31. B. Loopstra and P. Boldrini, *Acta Crystallographica*, 1966, 21, 158-162.
32. B. Loopstra and H. Rietveld, *Acta Crystallographica Section B: Structural Crystallography and Crystal Chemistry*, 1969, 25, 1420-1421.
33. G. Kresse and J. Furthmüller, *Computational Materials Science*, 1996, 6, 15-50.
34. G. Kresse and J. Furthmüller, *Physical Review B*, 1996, 54, 11169.
35. G. Kresse and D. Joubert, *Physical Review B*, 1999, 59, 1758.
36. B. Wang, J. Iqbal, X. Shan, G. Huang, H. Fu, R. Yu and D. Yu, *Materials Chemistry and Physics*, 2009, 113, 103-106.
37. J. P. Perdew and W. Yue, *Physical Review B*, 1986, 33, 8800.
38. A. Ehsani, M. G. Mahjani and M. Jafarian, *Turkish Journal of Chemistry*, 2011, 35, 735-743.
39. R. Jiang and D. Chu, *Electrochimica acta*, 2000, 45, 4025-4030.

40. M. Pourbaix, 1974.

41. T. Bligaard and J. K. Nørskov, *Electrochimica Acta*, 2007, 52, 5512-5516.

42. B. Hammer and J. K. Nørskov, *Advances in catalysis*, 2000, 45, 71-129.

43. M. Rubel, R. Haasch, P. Mrozek, A. Wieckowski, C. De Pauli and S. Trasatti, *Vacuum*, 1994, 45, 423-427.

44. D. D. Sarma and C. N. R. Rao, *Journal of Electron Spectroscopy and Related Phenomena*, 1980, 20, 25-45.

45. A. Katrib, F. Hemming, P. Wehrer, L. Hilaire and G. Maire, *Journal of Electron Spectroscopy and Related Phenomena*, 1995, 76, 195-200.

46. X. Li, F. Li, C. Yang and W. Ge, *Journal of Photochemistry and Photobiology A: Chemistry*, 2001, 141, 209-217.

47. K. Kadakia, M. K. Datta, O. I. Velikokhatnyi, P. Jampani, S. K. Park, P. Saha, J. A. Poston, A. Manivannan and P. N. Kumta, *International Journal of Hydrogen Energy*, 2012, 37, 3001-3013.

48. R. Bhattacharjee and I. M. Hung, *Materials Chemistry and Physics*, 2014, 143, 693-701.

Table 1: Results of electrochemical characterization for HOR of $(W_{1-x}Ir_x)O_y$ and Pt/C

Electro-catalyst	Onset potential (mV *vs* NHE)	Current density at 0 V (*vs* NHE) (mA cm^{-2})
$(W_{0.8}Ir_{0.2})O_y$	-27.41	0.42

$(W_{0.7}Ir_{0.3})O_y$	-43.55	0.73
WO_3	11.01	~0
IrO_2	-17.67	0.55
Pt/C	-25.7	0.71

827

828 **Table 2: Results of EIS analysis carried out at 0.016 V (*vs* NHE) in frequency range of**

829 **100 mHz-100 kHz and Tafel slope of $(W_{1-x}Ir_x)O_y$ and Pt/C**

Electro-catalyst	**R_Ω (Ωcm^2)**	**R_{ct} (Ωcm^2)**	**Tafel slope (mV/dec)**
WO_3	14.58	37	-
$(W_{0.8}Ir_{0.2})O_y$	14.21	30	71
$(W_{0.7}Ir_{0.3})O_y$	14.26	12.1	66
IrO_2	14.56	16.2	69
Pt/C	14.54	13.0	67.2

830

831 **Table 3: Results of polarization study of $(W_{1-x}Ir_x)O_y$ on RDE**

Electro-catalyst	**n**	**Kinetic current density, i_k (mA cm^{-2})**
$(W_{0.7}Ir_{0.3})O_y$	1.81	3.71
Pt/C	1.80	3.41

832

Figure captions:

Figure 1: The XRD pattern of WO_3, $(W_{1-x}Ir_x)O_y$ (x=0.2, 0.3) and IrO_2 nanoparticles in wide angle 2θ scan.

Figure 2: (a) The cyclic voltammetry (CV) curves for HOR of WO_3-NPs, IrO_2-NPs and Pt/C, measured in H_2 saturated 0.5 M H_2SO_4 at 40^0C at scan rate of 10 mV/sec, (b) The linear scan voltammogram (LSV) curves for HOR of WO_3-NPs, IrO_2-NPs and Pt/C, measured in H_2 saturated 0.5 M H_2SO_4 at 40^oC at scan rate of 10mV/sec, before and after iR_Ω correction.

Figure 3: The variation of current density *vs* time in the chronoamperometry test of WO_3-NPs, IrO_2-NPs and Pt/C, performed in a 0.5 M H_2SO_4 solution under a constant potential of ~0.016 V (*vs* NHE) at 40^oC for 24 h.

Figure 4: The projected density of d-electronic states calculated for $(W_{0.75}Ir_{0.25})O_y$ composition along with Pt and the projected d-Ir and d-W components of the densities of electronic states for $(W_{0.75}Ir_{0.25})O_y$. Arrows denote position of d-band centers $\varepsilon_{d.}$

Figure 5: The bright field TEM image of $(W_{0.7}Ir_{0.3})O_y$.

Figure 6: (a) SEM micrograph with elemental mapping of $(W_{0.7}Ir_{0.3})O_y$, (b) EDAX spectrum of $(W_{0.7}Ir_{0.3})O_y$.

Figure 7: The XPS spectra of WO_3, IrO_2 and $(W_{0.7}Ir_{0.3})O_y$ showing (a) Ir $4f_{5/2}$ and $4f_{7/2}$ doublet, (b) W $4f_{5/2}$ and $4f_{7/2}$ doublet and (c) O 1s peak.

Figure 8: (a) The cyclic voltammetry (CV) curves for HOR of WO_3 and $(W_{1-x}Ir_x)O_y$ (x=0.2, 0.3), measured in H_2 saturated 0.5 M H_2SO_4 at 40^0C at scan rate of 10 mV/sec, (b) The linear scan voltammogram (LSV) curves for HOR of WO_3 and $(W_{1-x}Ir_x)O_y$ (x=0.2, 0.3) and Pt/C, measured in H_2 saturated 0.5 M H_2SO_4 at 40^oC at scan rate of 10 mV/sec, before and after iR_Ω

correction, (c) Variation of onset potential and current density (at 0 V *vs* NHE) with iridium content.

Figure 9: EIS spectra of WO_3, $(W_{1-x}Ir_x)O_y$ (x=0.2, 0.3), IrO_2 and Pt/C obtained at ~0.016 V (*vs* NHE) in 0.5 M H_2SO_4 at 40^0C in the frequency range of 100 mHz-100 kHz.

Figure 10: The linear scan voltammogram (LSV) curve for HOR of $(W_{0.7}Ir_{0.3})O_y$ obtained on rotating disk electrode (RDE), measured in H_2 saturated 0.5 M H_2SO_4 solution at 40^oC with scan rate of 10 mV/sec. Koutechy-Levich plot of $(W_{0.7}Ir_{0.3})O_y$ is shown in inset of LSV curve.

Figure 11: (a) The variation of current density *vs* time in the chronoamperometry test of $(W_{0.7}Ir_{0.3})O_y$, and Pt/C, performed in a 0.5 M H_2SO_4 solution under a constant potential of ~0.016 V (*vs* NHE) at 40^0C for 24 h, (b) The cyclic voltammetry (CV) curve for HOR of $(W_{0.7}Ir_{0.3})O_y$ and Pt/C, measured in H_2 saturated 0.5 M H_2SO_4 at 40^oC at scan rate of 10 mV/sec, obtained after 24 h chronoamperometry test.

Figure 12: (a) Performance of single PEMFC (initial and after 24 h of operation) with $(W_{0.7}Ir_{0.3})O_y$ (total loading=0.2 mg cm^{-2}) and (b) Pt/C (0.2 mg of Pt cm^{-2}) as anode electro-catalyst and Pt/C (0.3 mg of Pt cm^{-2}) as cathode electro-catalyst at 80^oC and 0.1 MPa with UHP-H_2 (200 ml/min) and UHP-O_2 (300 ml/min) as reactant gases.

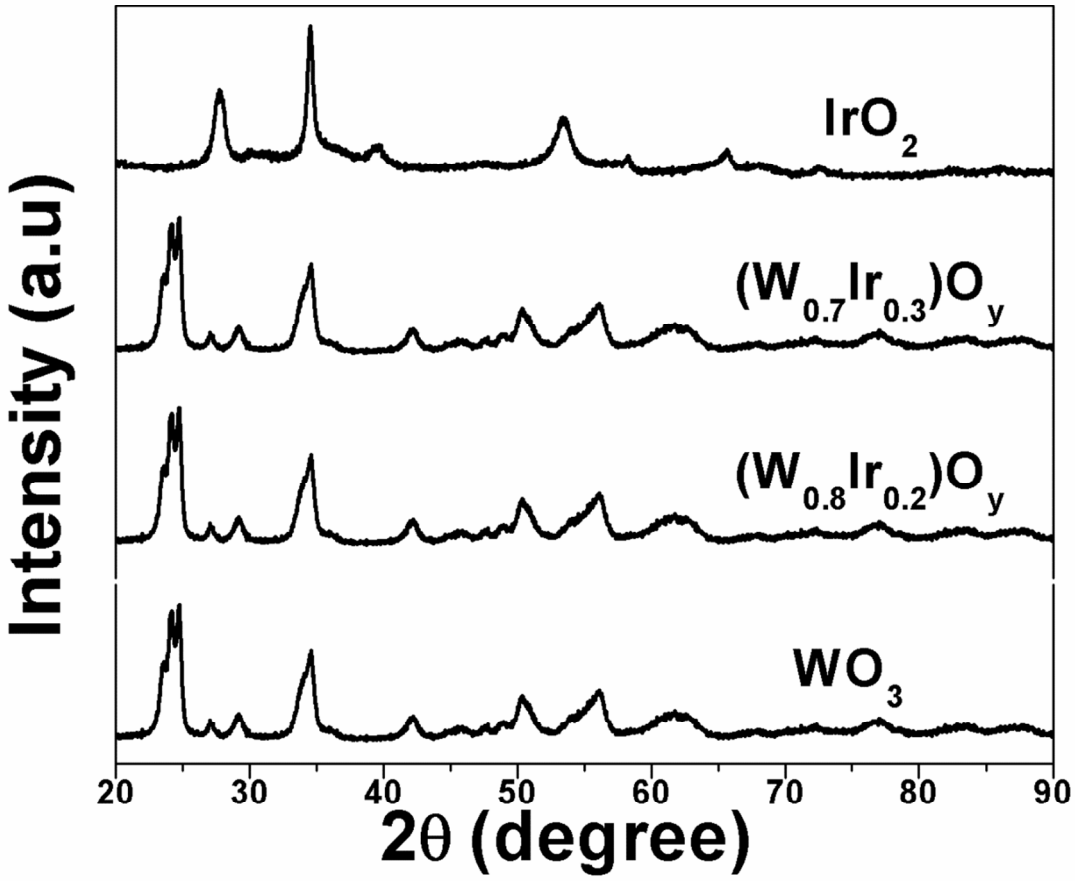

871

872 **Figure 1**

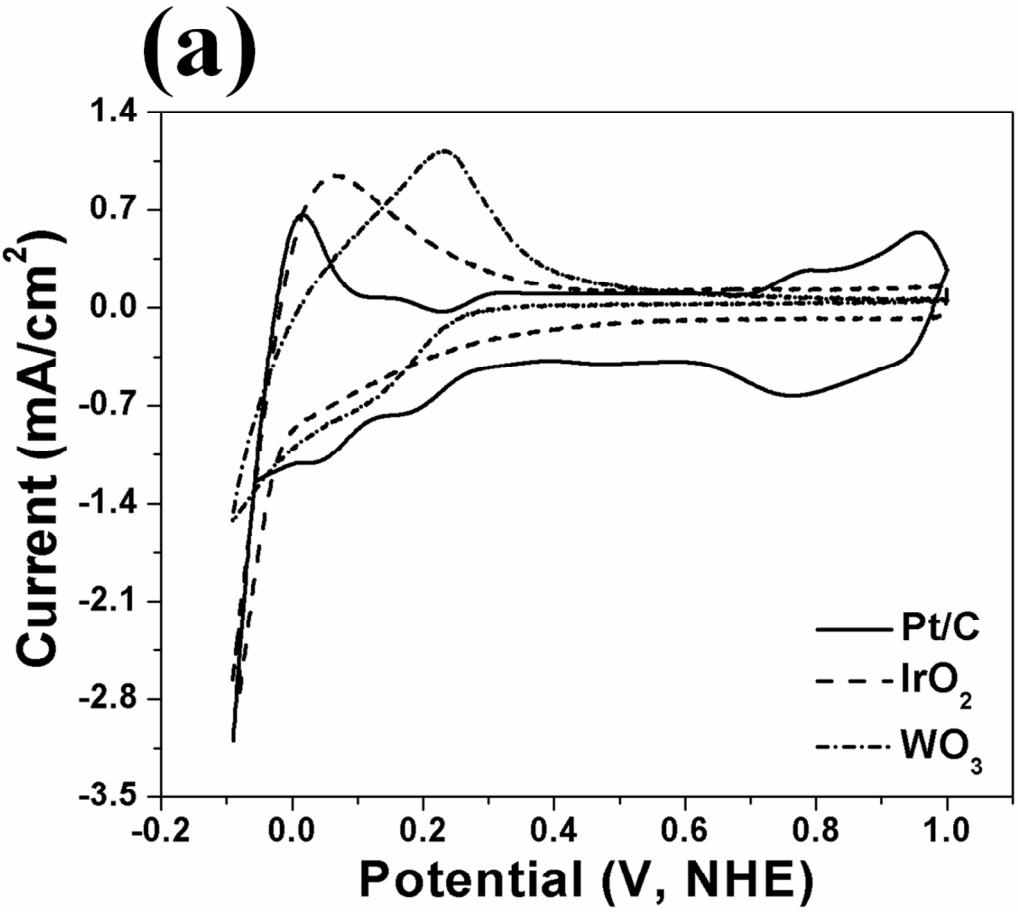

873

874 **Figure 2a**

875

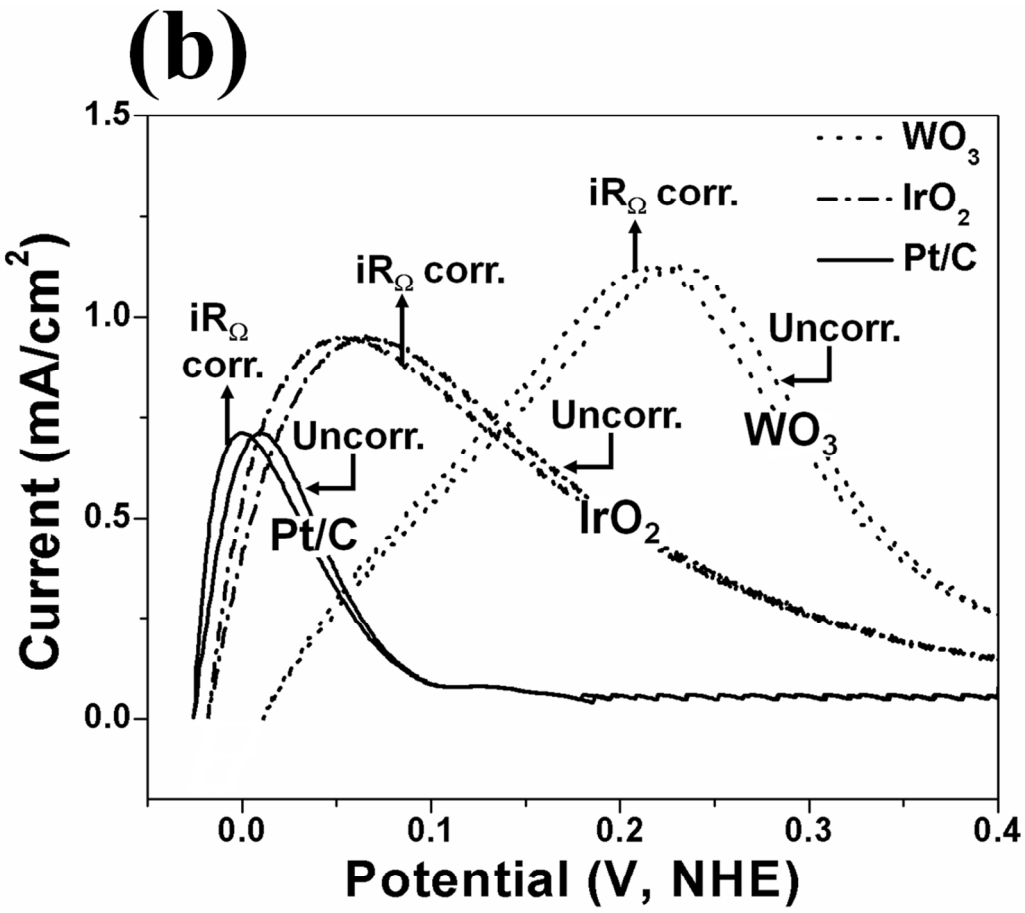

876

877 **Figure 2b**

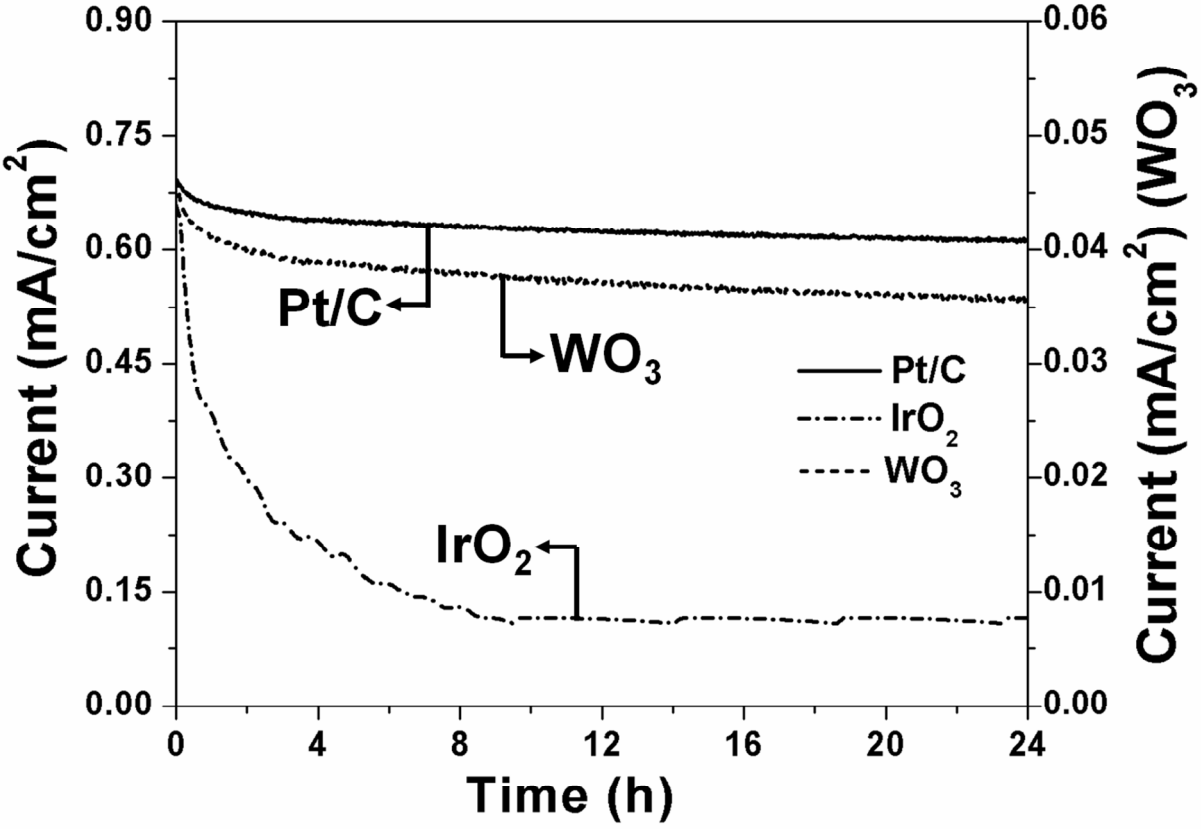

878

879 **Figure 3**

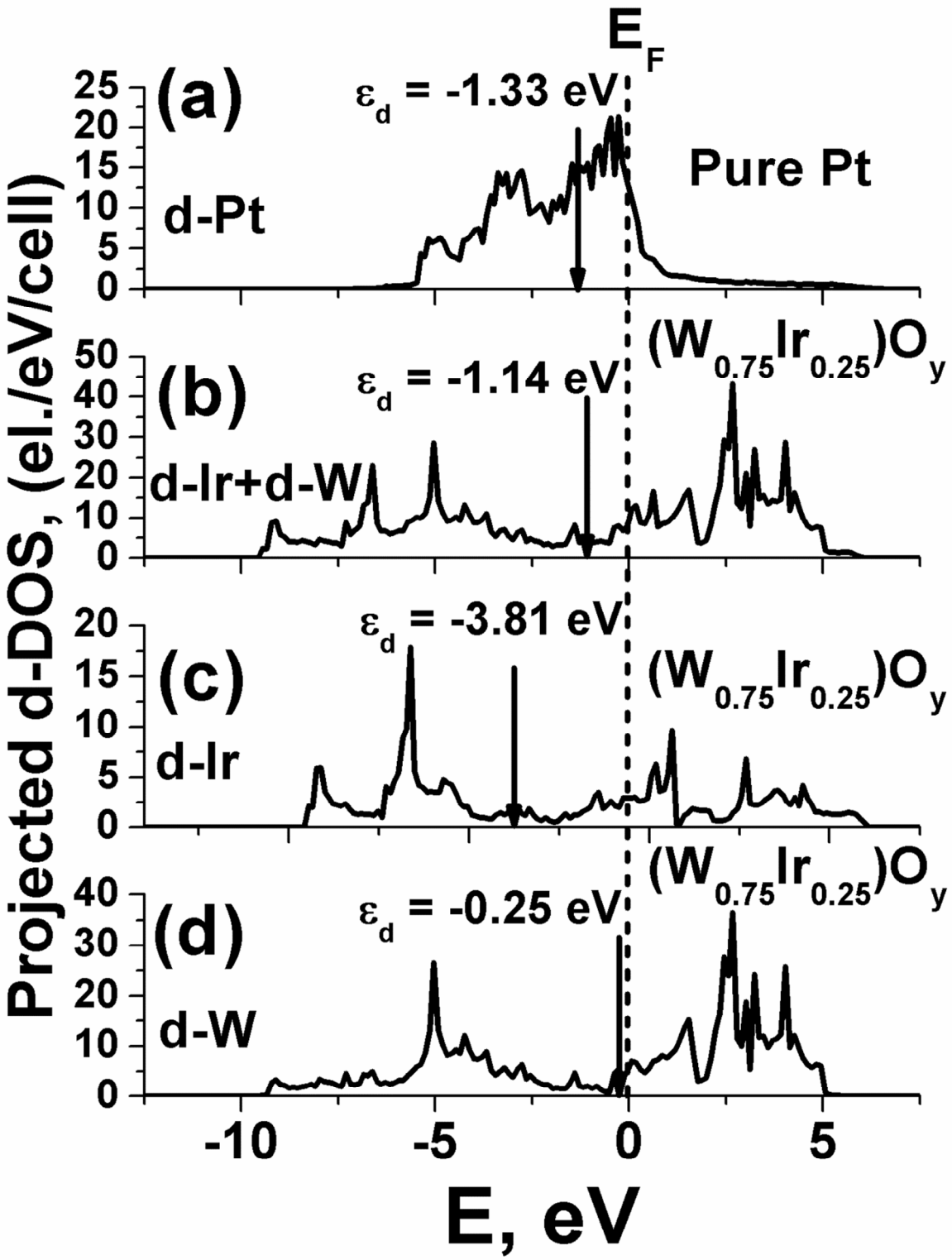

880

881 **Figure 4**

882

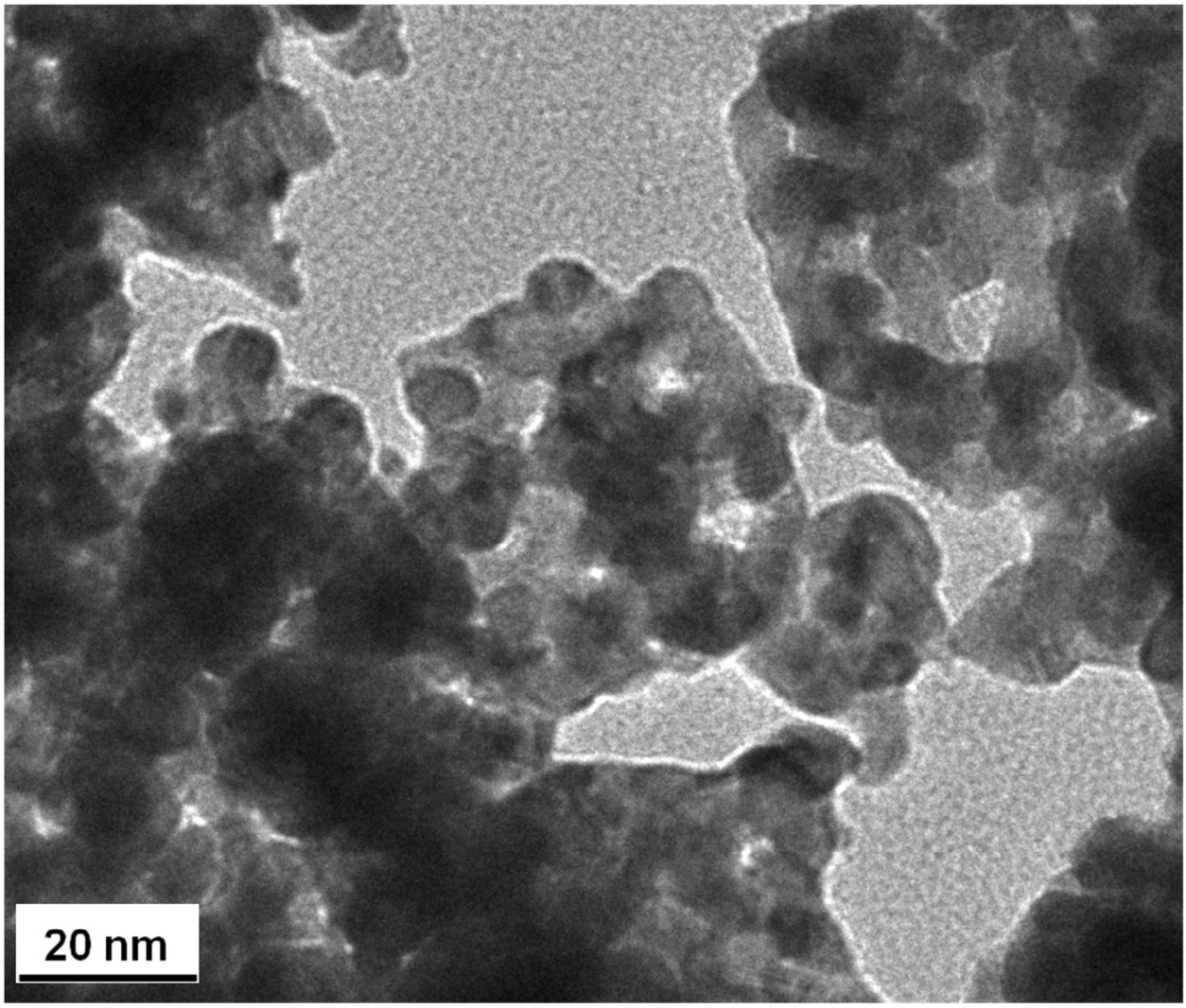

883

884 **Figure 5**

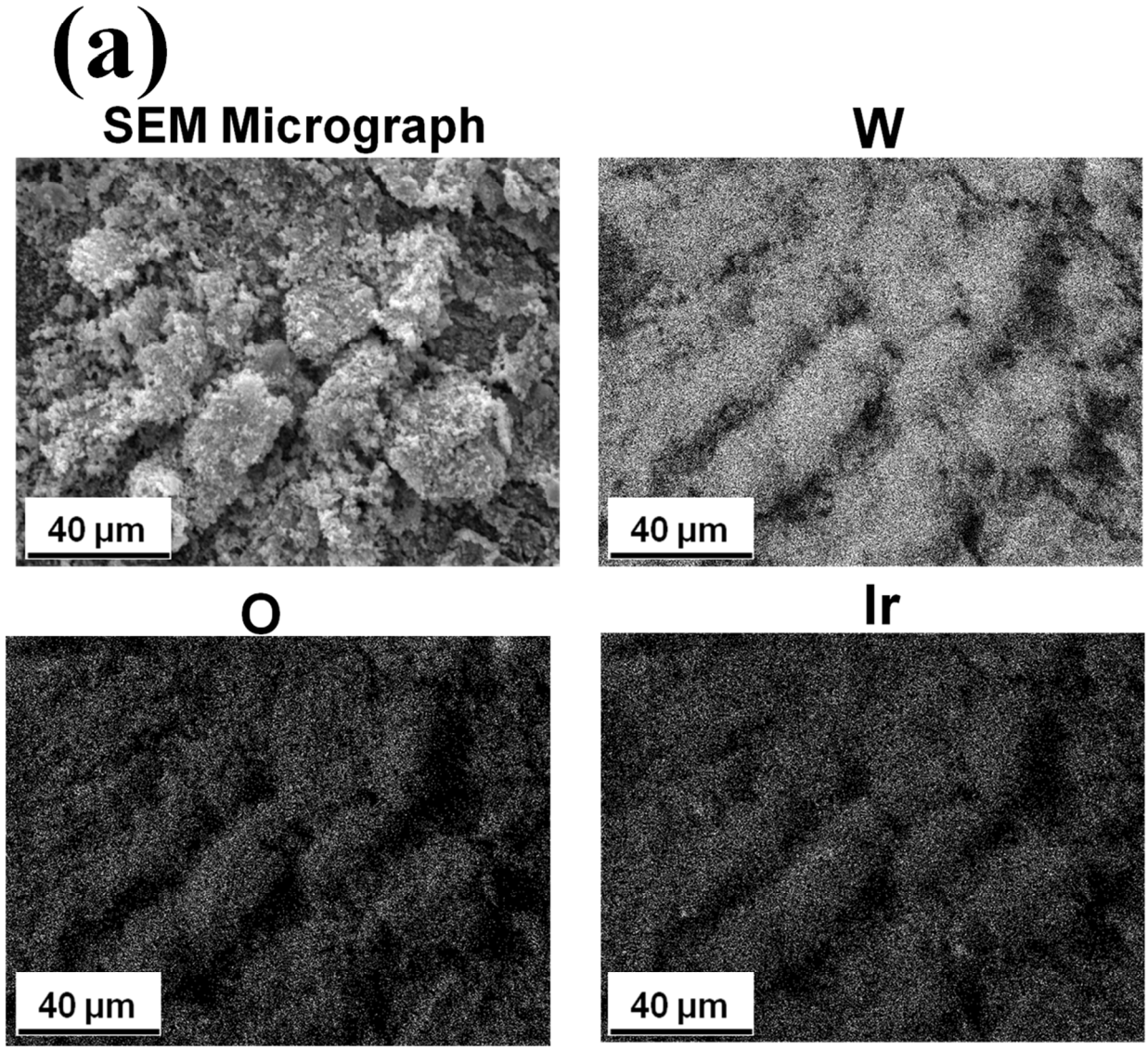

885

886 **Figure 6a**

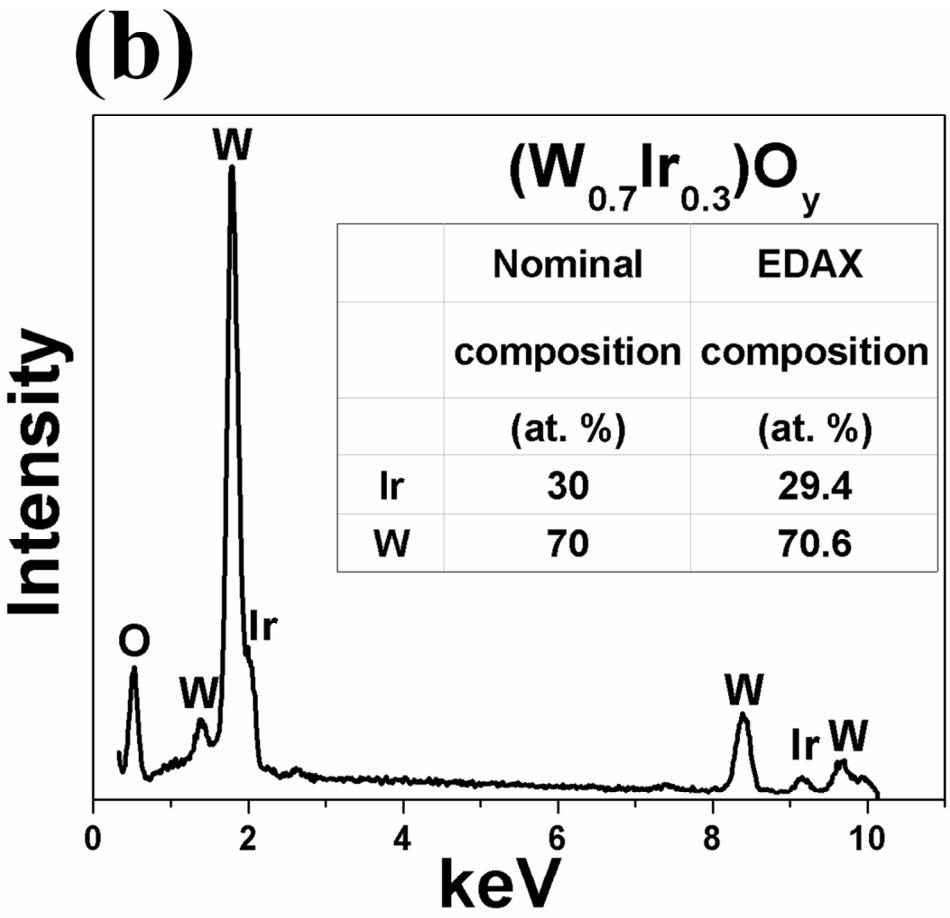

887

888 **Figure 6b**

889

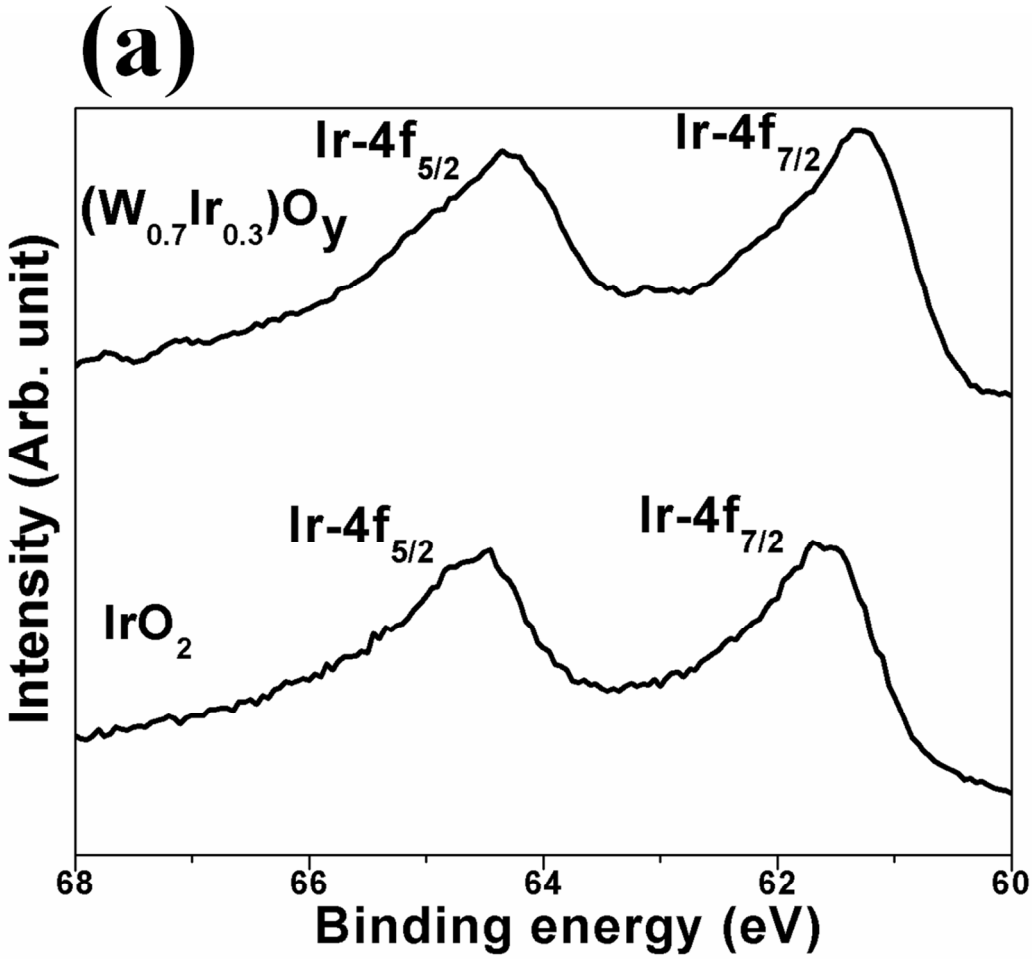

890

891 **Figure 7a**

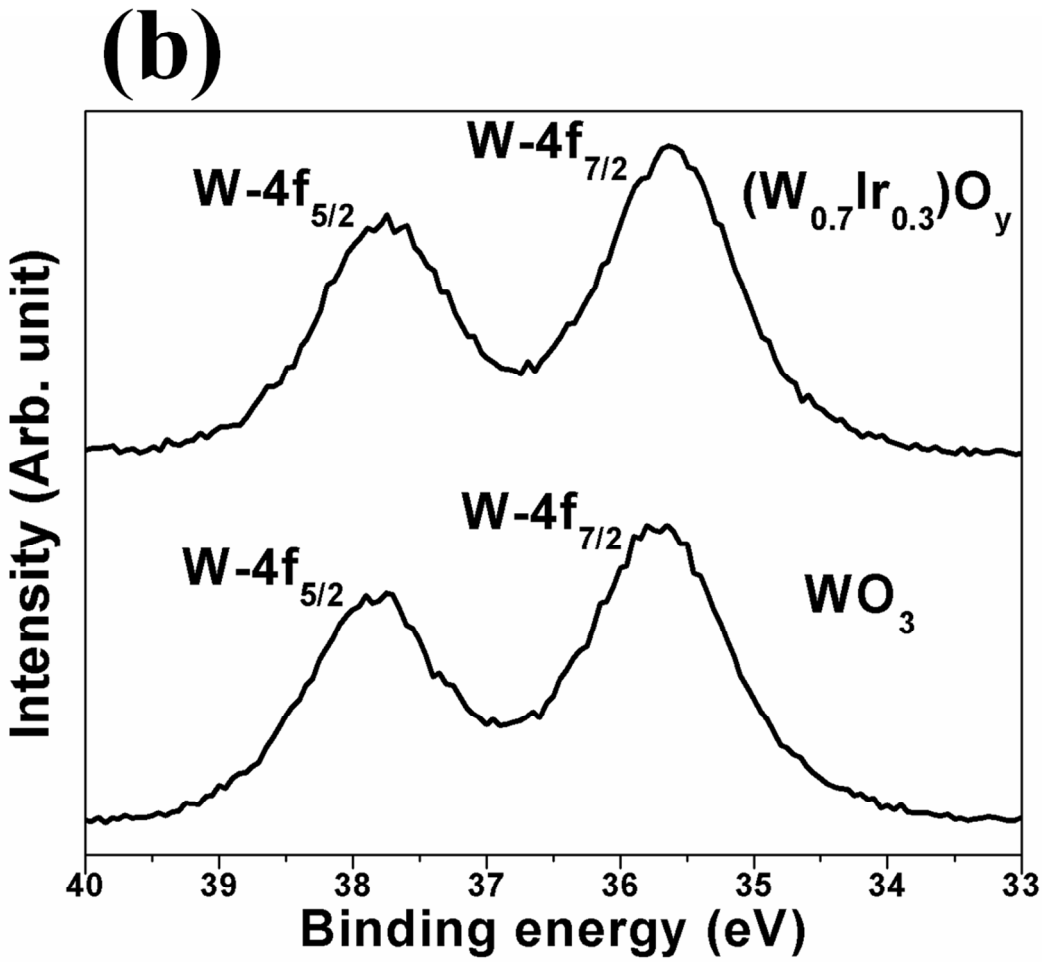

892

893 **Figure 7b**

894

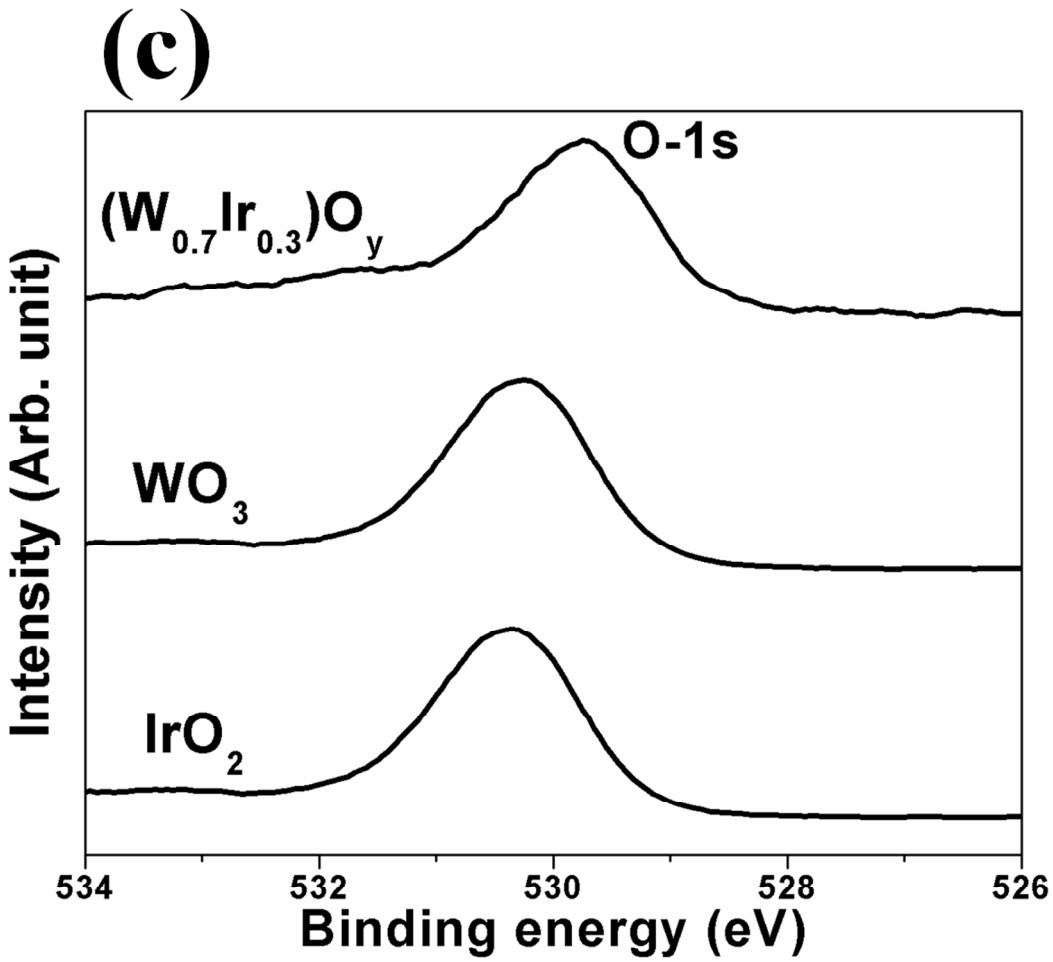

895

896 **Figure 7c**

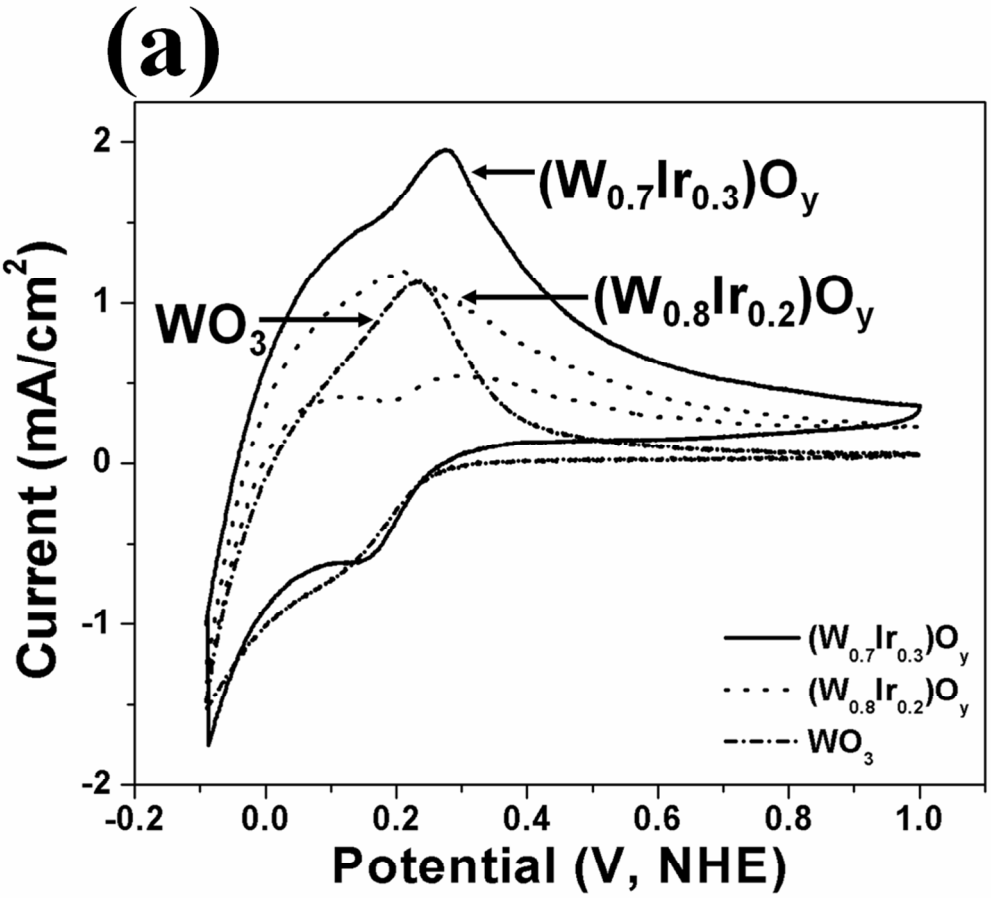

897

898 **Figure 8a**

899

900

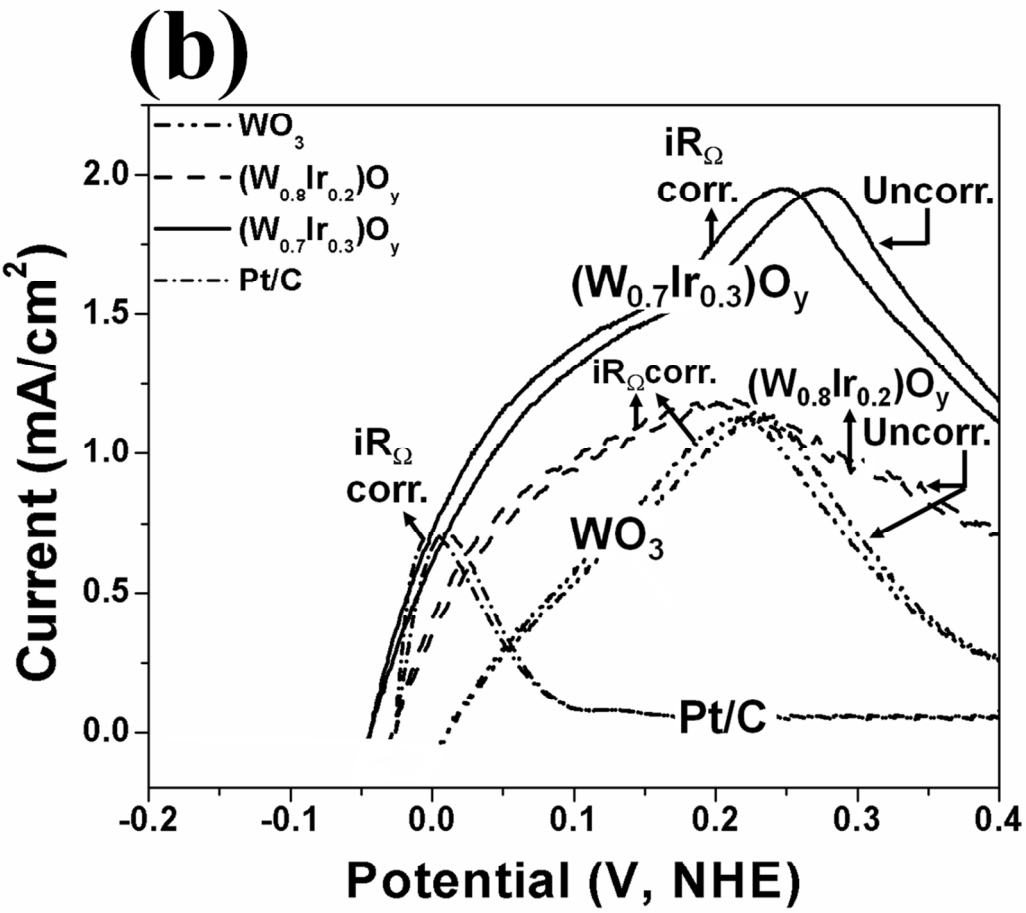

901

902 **Figure 8b**

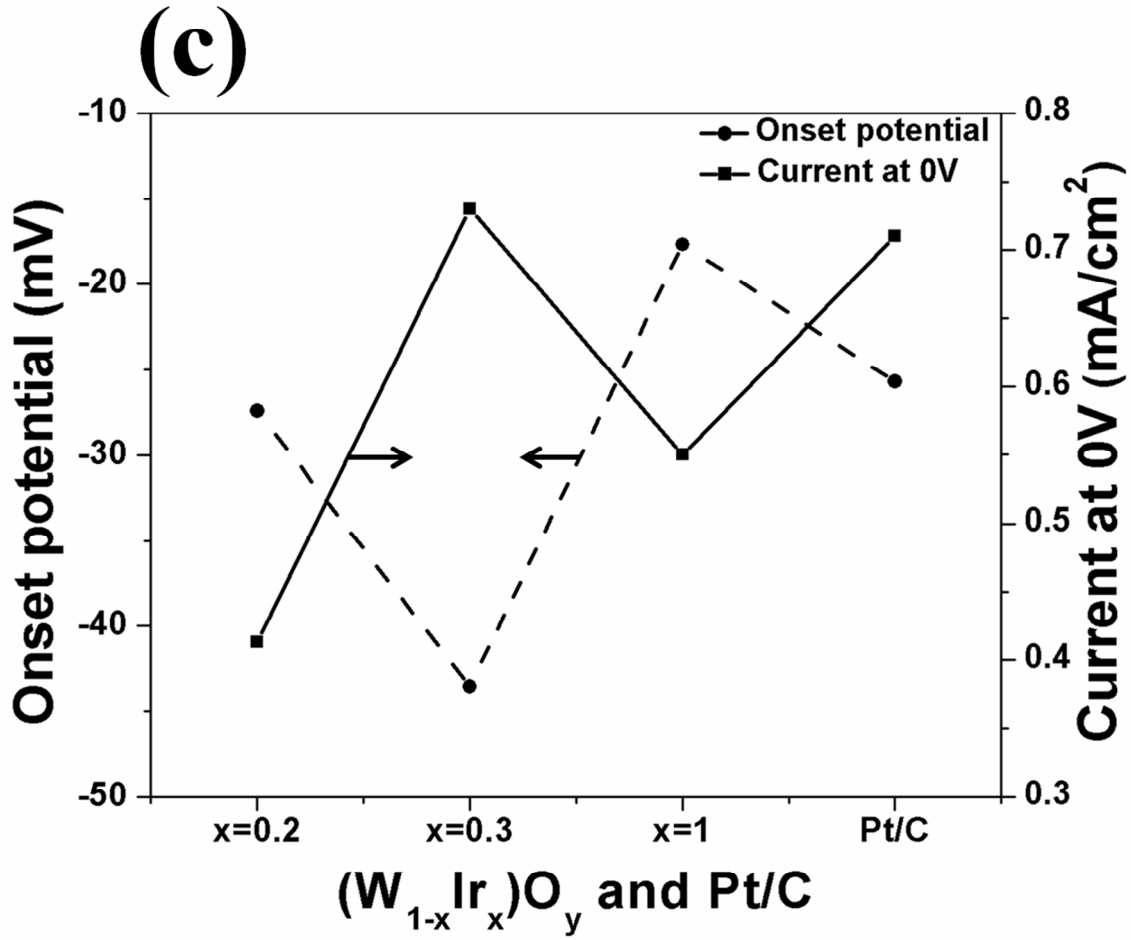

903

904 **Figure 8c**

905

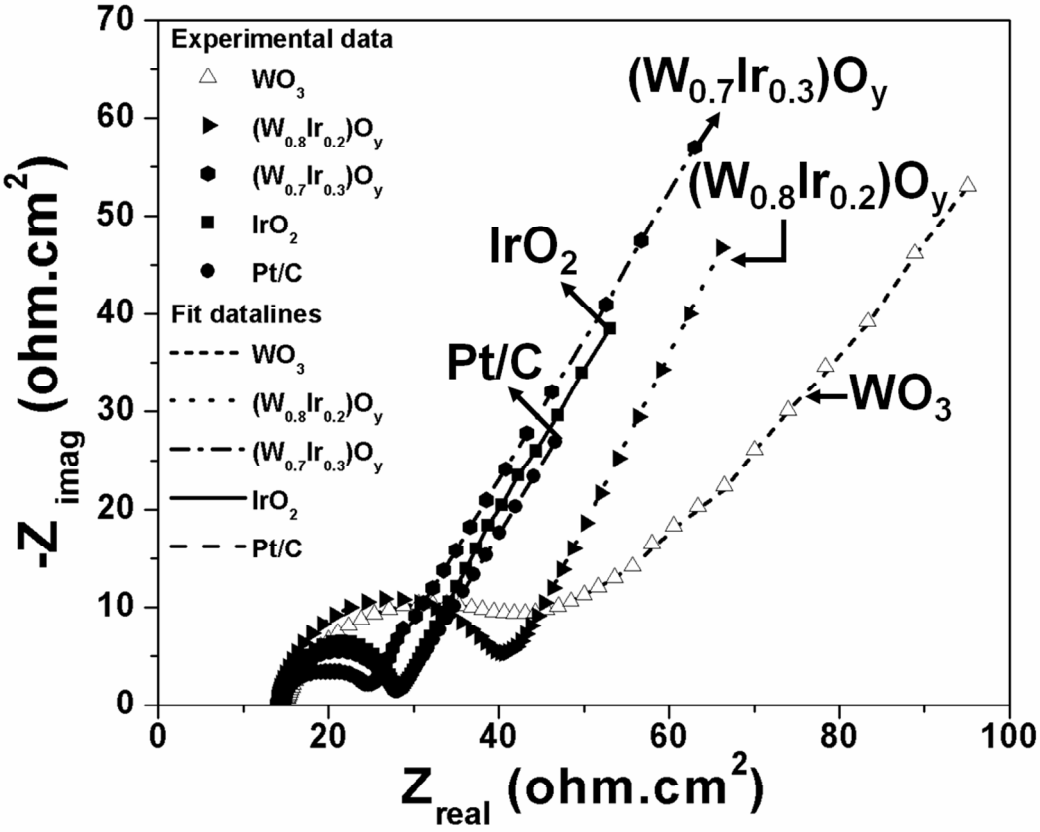

906

907 **Figure 9**

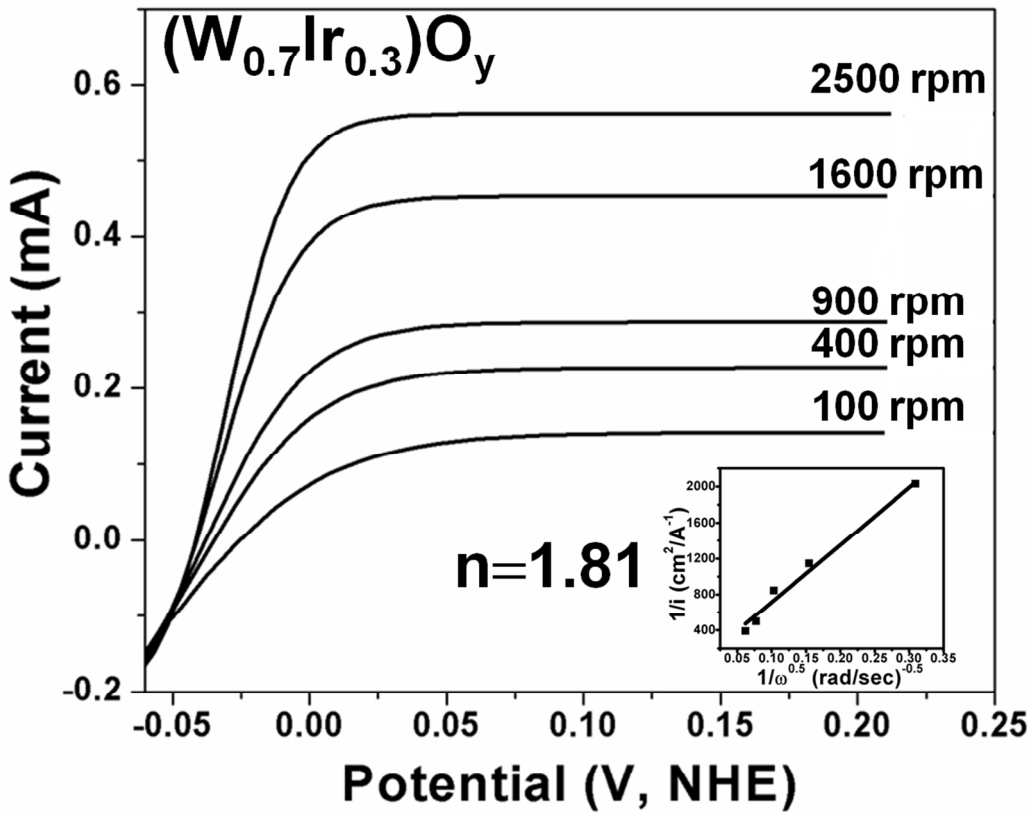

908

909 **Figure 10**

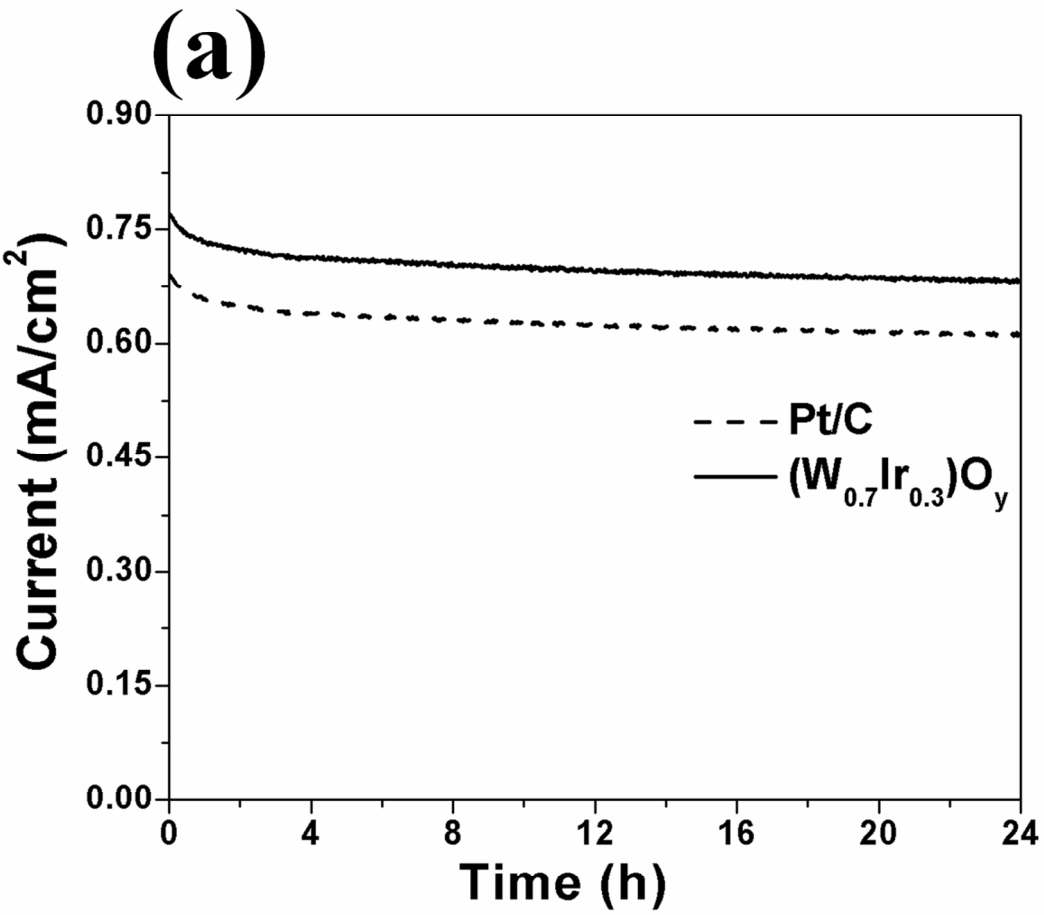

910

911 **Figure 11a**

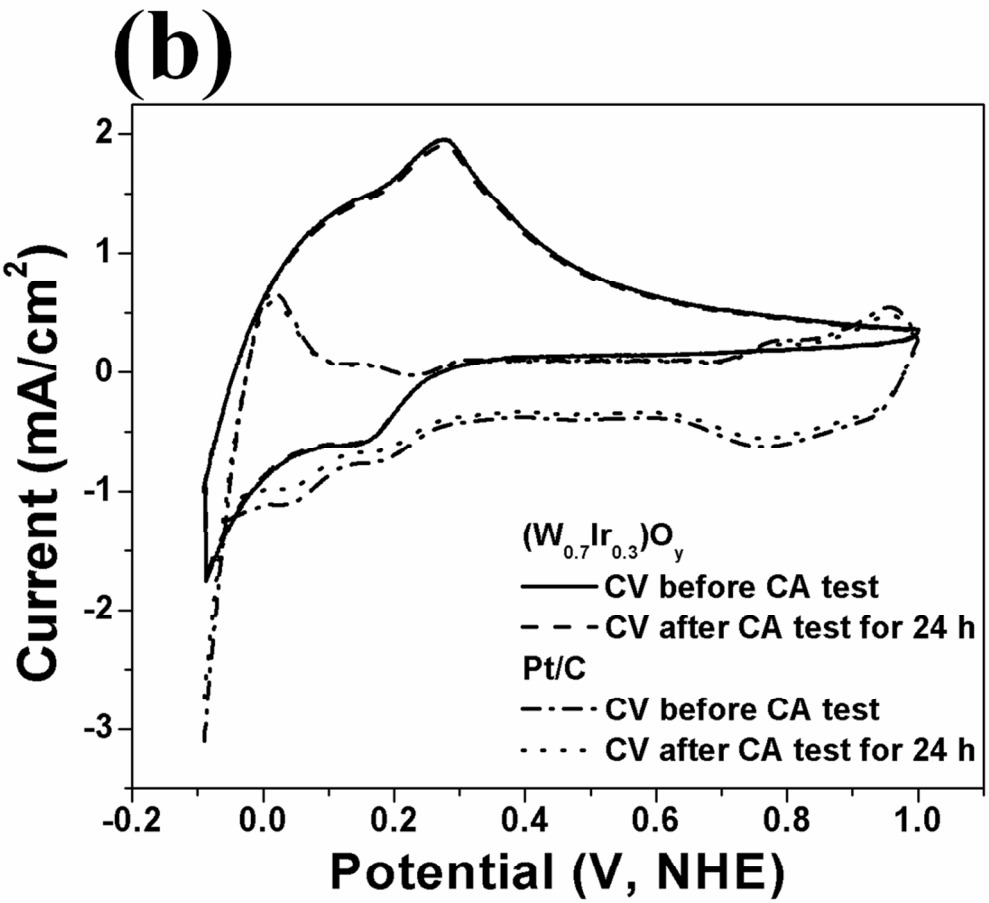

912

913 **Figure 11b**

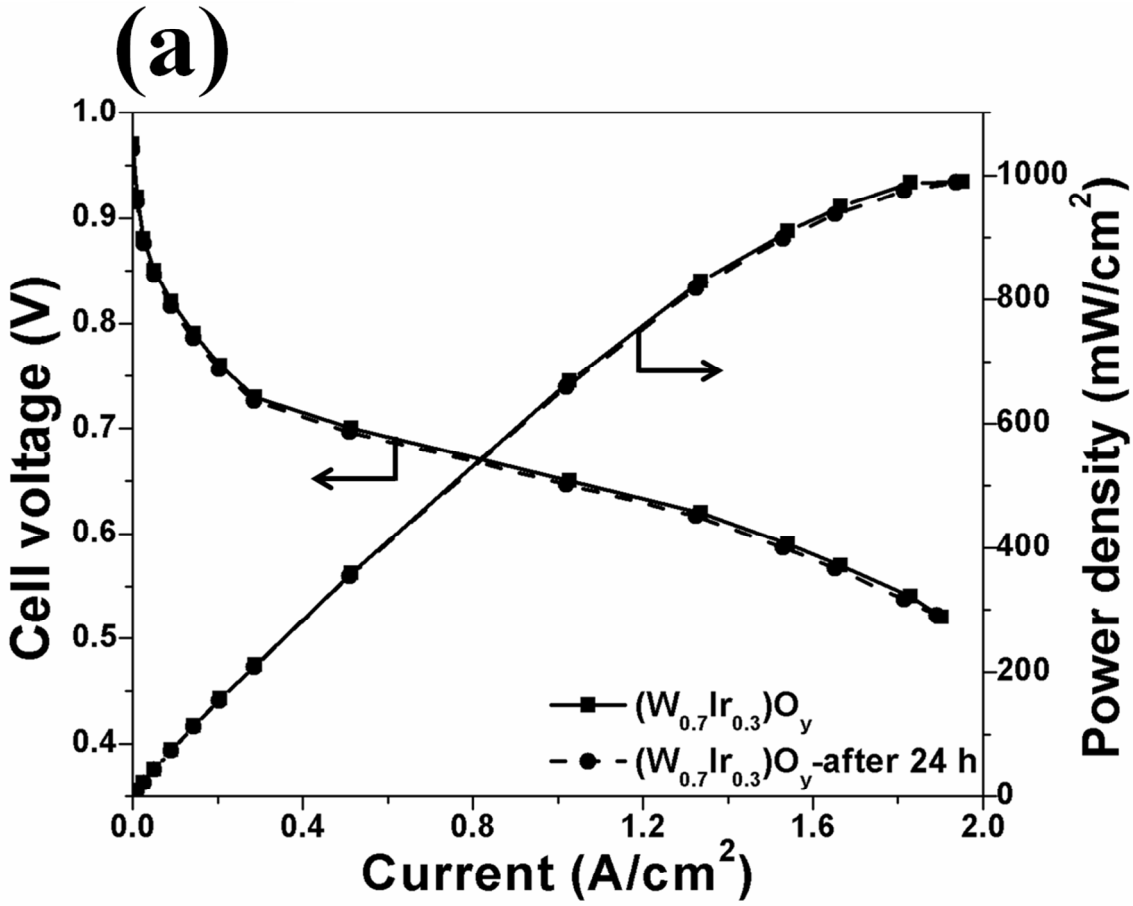

914

915 **Figure 12a**

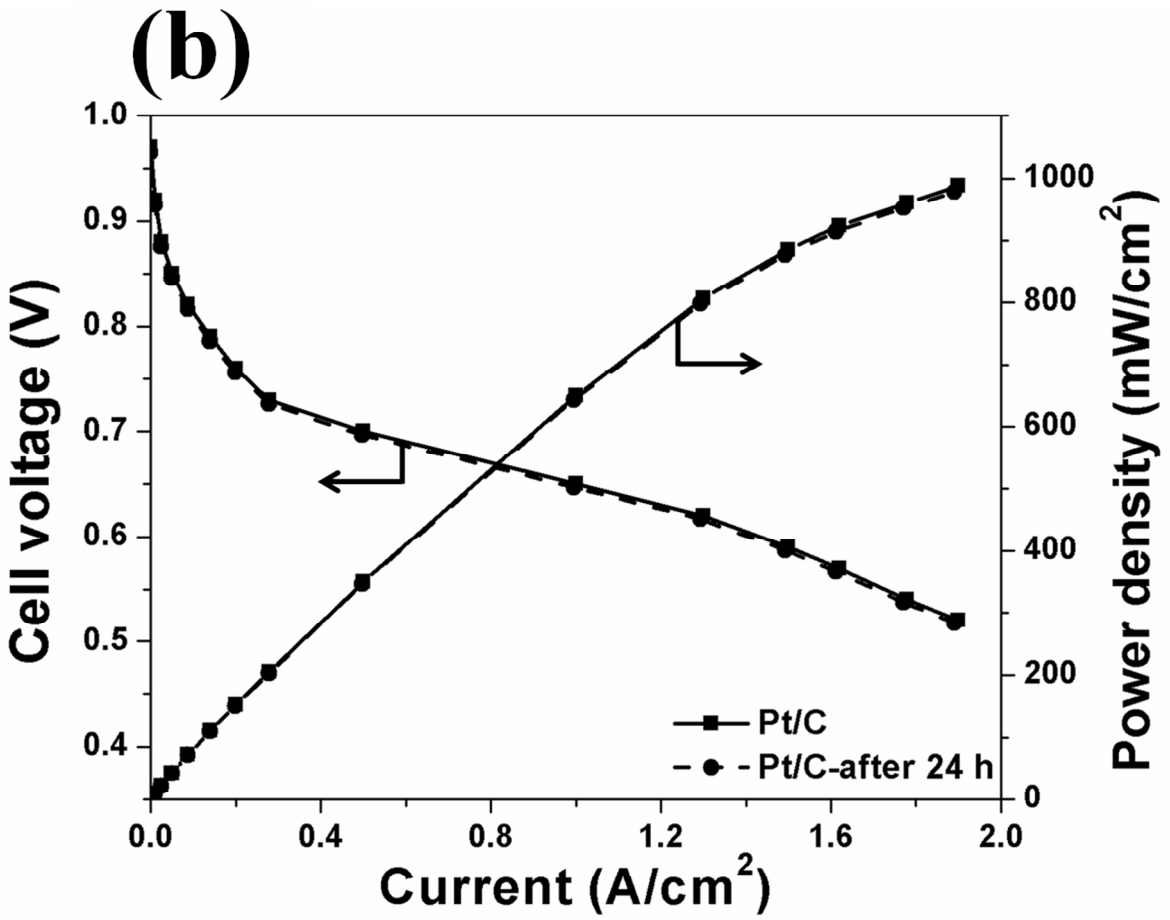

Figure 12b

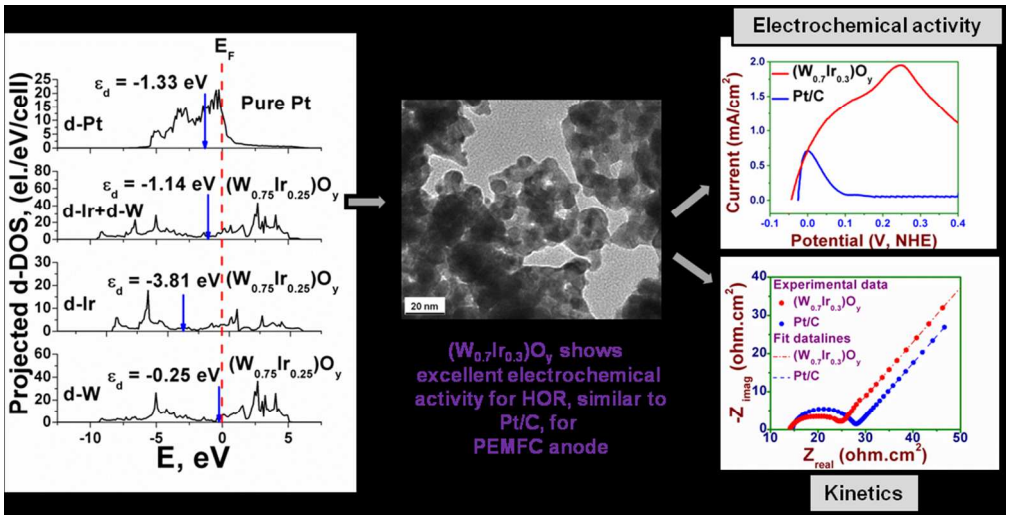

192x97mm (150 x 150 DPI)